INSTITUT FÜR AERODYNAMIK
UND GASDYNAMIK

Direktor: Prof. Dr.-Ing. F. X. Wortmann
UNIVERSITÄT STUTTGART · PFAFFENWALDRING 21 · 7000 STUTTGART 80 (VAIHINGEN)

Telefon: (07 11) 78 41; Durchwahl: 784.....

AIRFOIL SYNTHESIS TECHNIQUES

F.X.Wortmann

Principal Lecturer at a One-Week Short Course on

"Optimum Design of Airfoils"

Department of Aerospace Engineering
The University of Texas at Arlington

April 5-9, 1976

Introduction

Airfoils are a special class of "streamlined" shapes which are able to produce large lift forces at the expense of small drag values. Selecting an airfoil for a certain engineering application has mostly been done in the past by comparing the qualities of different airfoils gathered in airfoil catalogues. Today the availability of a large body of knowledge and of fast computers has changed the situation.

However, the old question: is this airfoil for this purpose nearly the best one, can very often not be answered because an airfoil is mostly a compromise between conflicting requirements. Because the number of possible modifications is infinite, it is certainly not enough to compare one solution with another one.

Considering modifications, we should know which way is the most promising, which gives the best, overall compromise and how close do we come to the physical limits? A deeper understanding of the flow phenomena and their interdependence is surely necessary for any decision.

It is hoped that the following compilation which contains some basic and simplified facts of the potential and boundary layer flow over two-dimensional airfoils may be helpful to select or synthesize improved and better adapted airfoils.

I. Boundary layer behaviour

a) Laminar flow

If we exclude strong turbulence of the freestream, excessive roughness on the surface or the turbulent contamination along a swept-back wing nose, then a boundary layer starts with a laminar state at the stagnation point even at very high Reynoldsnumbers. For instance, it is hard to get turbulence in front of the instability point and on a conventional airfoil of medium thickness this point lies at $Re_c = 10^8$ between 4-6% chord. It needs only a smooth surface and a suitable pressure distribution to ensure a reliably laminar flow far beyond the instability point.

In order to get a quick impression of the boundary layer, we remember for the momentum thickness the wellknown formula of Walz (1) or Thwaites (2)

$$\left(\frac{\vartheta}{c}\right)^2 = \frac{.47}{\left(\frac{u}{u_\infty}\right)^6 Re_c} \int_0^{x/c} \left(\frac{u}{u_\infty}\right)^5 d\frac{x}{c} \qquad (1)$$

and

$$\Gamma = \left(\frac{\vartheta}{c}\right)^2 Re_c \cdot \frac{d\frac{u}{u_\infty}}{d\frac{x}{c}} \qquad (2)$$

for the shape parameter.

Very often it is easy to approximate the velocity in the front part of the airfoil by distribution of the type

$$\frac{u}{u_\infty} = \alpha \left(\frac{x}{c}\right)^m \qquad (3)$$

Such velocities produce so-called similar sclutions with constant shape parameters. The momentum thickness now becomes

$$\left(\frac{\vartheta}{c}\right)^2 = \frac{A \cdot \frac{x}{c}}{\frac{u}{u_\infty} Re_c} \qquad (4)$$

The constants of Equ.(1) are in Equ.(4) slightly changed to improve the accuracy with respect to the exact Hartree solution:

$$A = \frac{.44}{1 + 4.165m} \qquad m < 0 \tag{5}$$

$$A = \frac{.44}{1 + 3.165m} \qquad m > 0$$

For airfoils the values of m are mostly between m = -0,09 for the separating boundary layer and m = 1 for the stagnation flow. Some values of A are given in Table 1 and show that the momentum thickness does not change very much in the case of an accelerating flow (m > 0).
The shape parameter is now independent of x/c.

Table I

m	A	A/A_o
1.0	.11	.~~105~~
.5	.170	.386
.1	.3342	.76
.05	.379	.86
0.	.44	1.0
- .05	.555	1.26
- .07	.618	1.40
- .09	.703	1.59

.25

$$\Gamma = A \cdot m \tag{6}$$

Since in boundary layer theory several shape parameters are used Fig.1 shows the relationship between $H_{12} = \frac{\delta^*}{\vartheta} = \frac{\delta_1}{\delta_2}$, $H_{32} = \frac{\delta^{**}}{\vartheta} = \frac{\delta_3}{\delta_2}$ Γ , and m. Typical points in Fig.1 are H_{32} = 1,572 (flat plate) and H_{32} = 1,515 (separation).

From (4) we get

$$re_\vartheta = \frac{\vartheta}{c} \cdot \frac{U}{U_\infty} \cdot Re_c$$

$$re_\vartheta^2 = A \cdot \frac{x}{c} \cdot \frac{U}{U_\infty} Re_c = A \alpha \left(\frac{x}{c}\right)^{1+m} Re_c \tag{7}$$

These simple formula give an immediate answer how the laminar boundary layer will develop on an airfoil when the velocity distribution is known.

Often there is an interest to prescribe a velocity distribution which produces certain boundary layer qualities. A typical example is given in Fig.2. In the front part the velocity is $U/U_\infty = U_1/U_\infty$ = const up to $x/c = x_1/c$. Now behind this point we want a boundary layer which runs with a constant shape parameter, say m = -.09 or Γ = -.068.

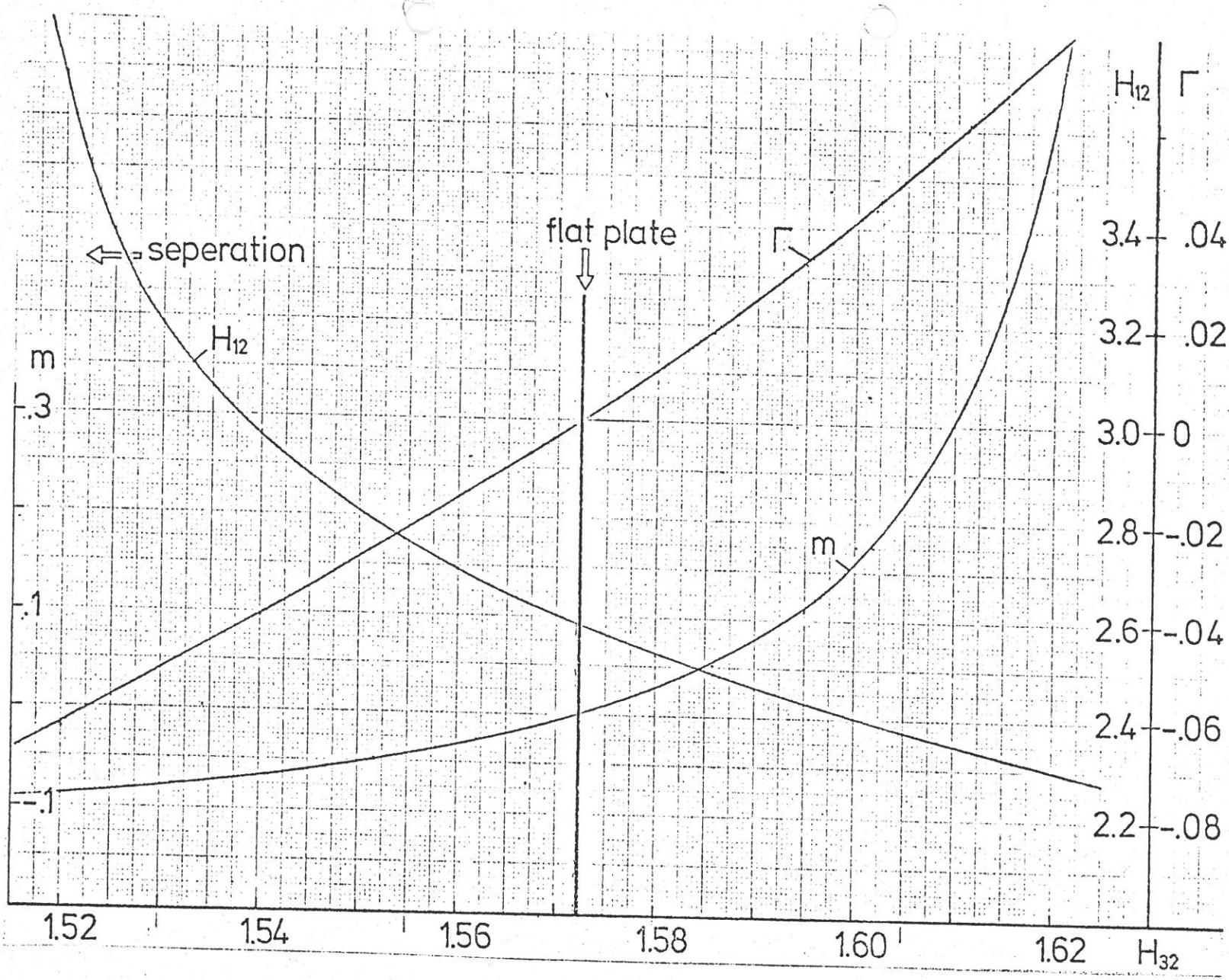

Fig.1 Different shape parameters of the laminar boundary layer as function of H_{32}.

The velocity

$$\frac{u}{u_\infty} = \alpha \left(\frac{\bar{x}}{c}\right)^{-.09} \tag{8}$$

with another length scale $\bar{x}$ yields such a boundary layer. To join both solutions at $x = x_1$, we need equal re_ϑ in x_1.

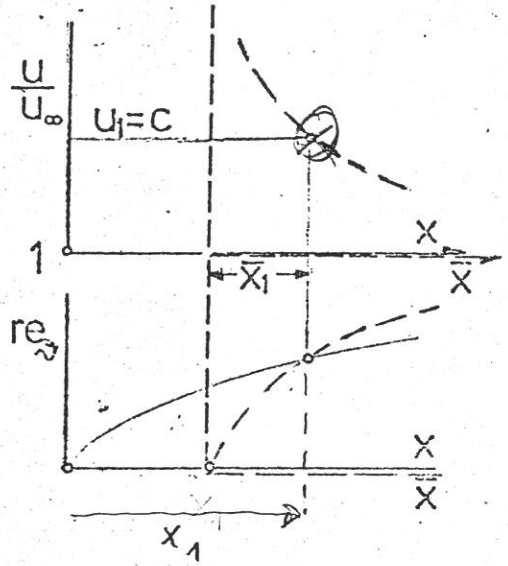

This condition requires a shift of the $\bar{x}$ scale:

$$\left(\frac{\bar{x}}{c}\right)_1 = (1 + 4.165\,m)\left(\frac{x}{c}\right)_1 \qquad m < 0 \tag{9}$$

and

$$\alpha = \frac{u_1/u_\infty}{\left(\frac{\bar{x}_1}{c}\right)^m}$$

and

$$\frac{\bar{x}}{c} = \frac{\bar{x}_1}{c} + \frac{\Delta x}{c} \qquad \frac{\Delta x}{c} = \frac{\bar{x}}{c} - \frac{\bar{x}_1}{c}$$

Equ.(8) and (9) describe a velocity distribution along which the boundary layer will everywhere separate.

b) Stability and transition

For subsonic flow the stability of a laminar boundary layer is well understood as long as the perturbations of the freestream or the surface are very small. Then the stability is only influenced by the Reynoldsnumber and the pressure gradient. In terms of boundary layer the momentum Reynoldsnumber and the shape parameter reflect this influence. Fig.3 shows a theoretical result which separates the unstable conditions above from the stable ones below the line.

For the flat plate momentum Reynoldsnumber and length Reynoldsnumber are connected by Equ.(7)

$$Re_x = \frac{u \cdot x}{\nu} = \frac{re_\vartheta^2}{\frac{u}{u_\infty}} \cdot 2.27 \tag{10}$$

Near the stagnation point the instability momentum Reynoldsnumber is nearly 50 times higher than on the flat plate. A similar solution with m = + .07, which resembles an airfoil nose region, yields $re_{\vartheta_{crit}} \approx 2000$ i.e. $Re_x \approx 10^7$. This shows the extreme sensitivity of the laminar stability due to the pressure gradient. The same fact is illustrated in Fig.4 for a 15% Joukowsky air-

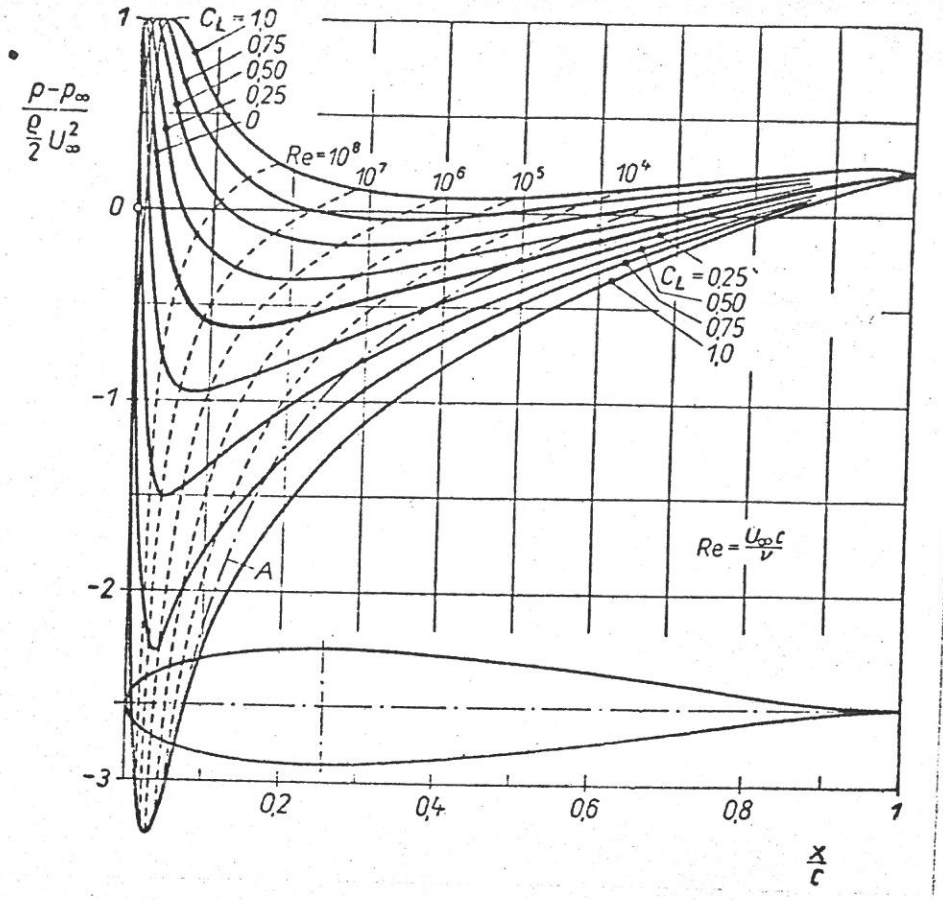

Fig.4 Pressure distribution, stability and separation of a Joukowsky airfoil

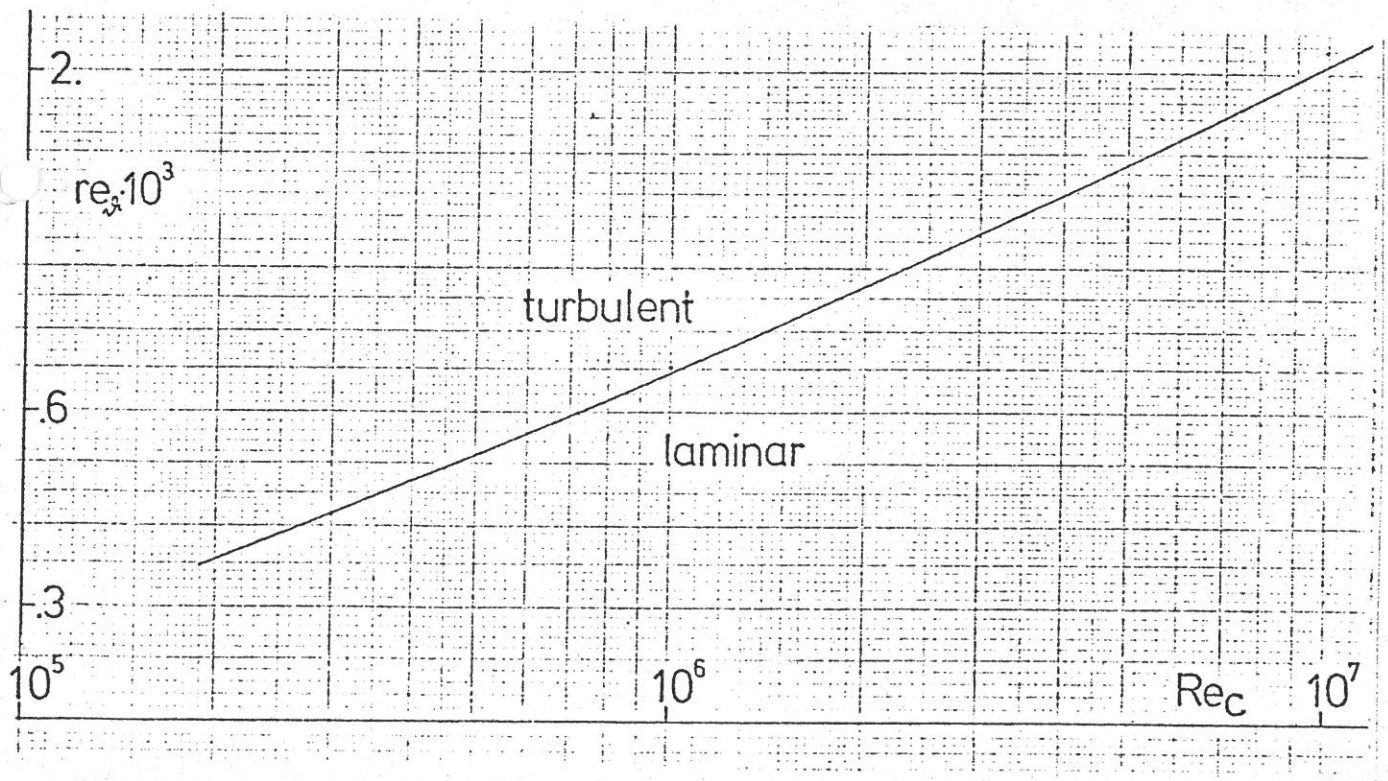

Fig.5 Michels transition criterion

foil at several C_L-values.

In contrast to the well established results of the linear stability theory which started nearly half a century ago the prediction of transition is still an open question and will be so in the future. The reason is very simple: the laminar boundary layer downstream the instability point is a strong amplifier for incoming perturbations. The amplification depends in the same way as the instability point on the boundary layer Reynoldsnumber and the pressure gradient or shape parameter. However, we do know neither the structure and size of these perturbations nor how they match with the amplifier characteristics, nor do we know the type and size of amplitude which finally yield turbulence.

There is enough experimental evidence to show that with smooth surfaces in the free atmosphere the amplification rate is rather high of the order $5 - 10 \cdot 10^3$. Due to the fact, that the amplification grows exponential in time or length, a high amplification rate implies very small changes in the transition length position, when the input amplitude is variable. A.M.O.Smith (3) and independently v.Ingen (3) have shown that the transition very often takes place when the amplification rate reaches values about e^9.

This is the basis of all of the so-called transition criteria which search for an empirical relationship for the position of transition as function of Re_x or re_ϑ and shape parameter.

Michel (4) has given an empirical relationship

$$re_{\vartheta(trans)} = 1.174 \left[1 + \frac{22.4}{Re_x} Re_x^{.46}\right] \qquad 10^5 < Re_x < 3 \cdot 10^7 \qquad (11)$$

which could be interpreted by A.M.O.Smith as a manifestation of the e^9 criterion, see Fig.5.

Another empirical criterion was given by Granville, see (3), who plotted the difference in re_ϑ between the instability and transition point as function of an average shape parameter between these points. His results which are based on experimental results in free flight or in low turbulence tunnels are included in Fig.3.

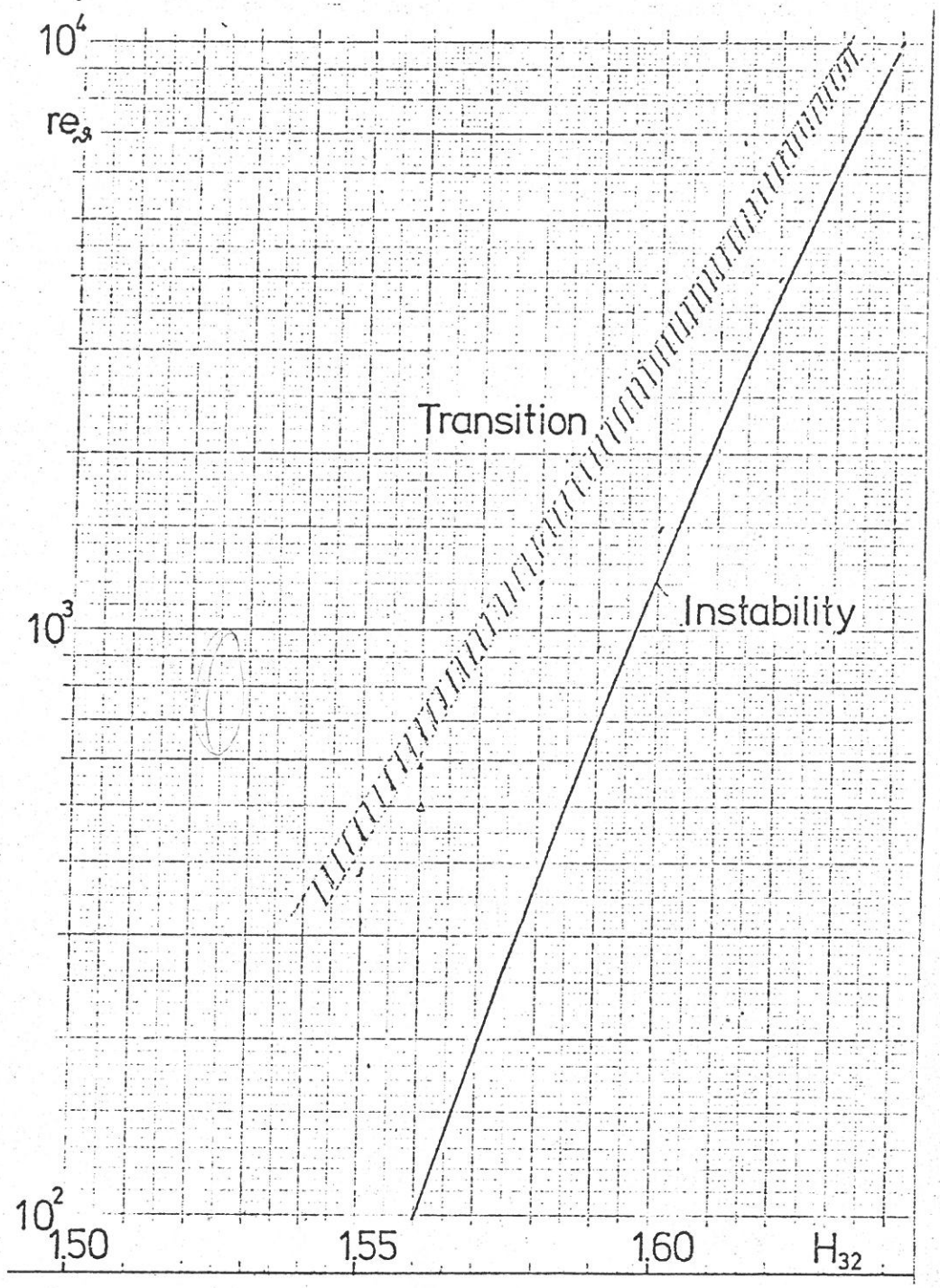

Fig.3 Stability and transition boundary as function of H_{32}

Fig.6 gives the values of $\frac{Re_\vartheta}{\sqrt{Re_c}}$ along the airfoil chord for $\alpha = 1$ and three m values. This figure can be used to get an impression how the velocity distribution can be used to control the transition position. The Granville criterion needs in the region of adverse pressure gradients a $\Delta Re_\vartheta \approx 400$. It can easily be seen, that even with a nearly separating laminar boundary layer it is difficult to produce at low Re_c-numbers a ΔRe_ϑ of 400. At $Re_c = 10^6$ more than half of the chord is needed for an instability range. We can draw the conclusion that for conventional airfoils with smooth surfaces and low freestream turbulence the transition will usually not take place in front of the separation point.

In this connection it may be useful to correct some observations of the famous NACA laminar airfoil developments in the forties: they were not able to verify laminar flow beyond length Reynolds numbers of $5\text{-}8 \cdot 10^6$. There are some later examples which show clearly that with low disturbances extremely high Reynolds numbers can be realized: on the flat plate Wells (5) from LTV observed transition at $5 \cdot 10^6$ in contrast to the $2{,}8 \cdot 10^6$ of Schubauer and Skramstad (3). W.Pfenninger verified laminar flow up to $1{,}3 \cdot 10^7$ in his suction experiments and Carmichael (6) demonstrated length Reynoldsnumbers of $1{,}6 \cdot 10^7$ on an underwater body.

The following conclusions can be made:

1) The pressure gradient has an overriding effect on the transition as long as the perturbations in the boundary layer are small. Such conditions are given for smooth surfaces and free flight in the atmosphere or deep sea.

2) When the pressure gradients before and behind the minimum point are not small ($|m| > .1$), the instability, separation and transition point are all close to the minimum, at least at $10^6 \leq Re_c \leq 10^7$.

3) When the pressure gradients are small the prediction of transition needs a criterion. Up to now, only a restricted information is available for low freestream turbulence and smooth surfaces.

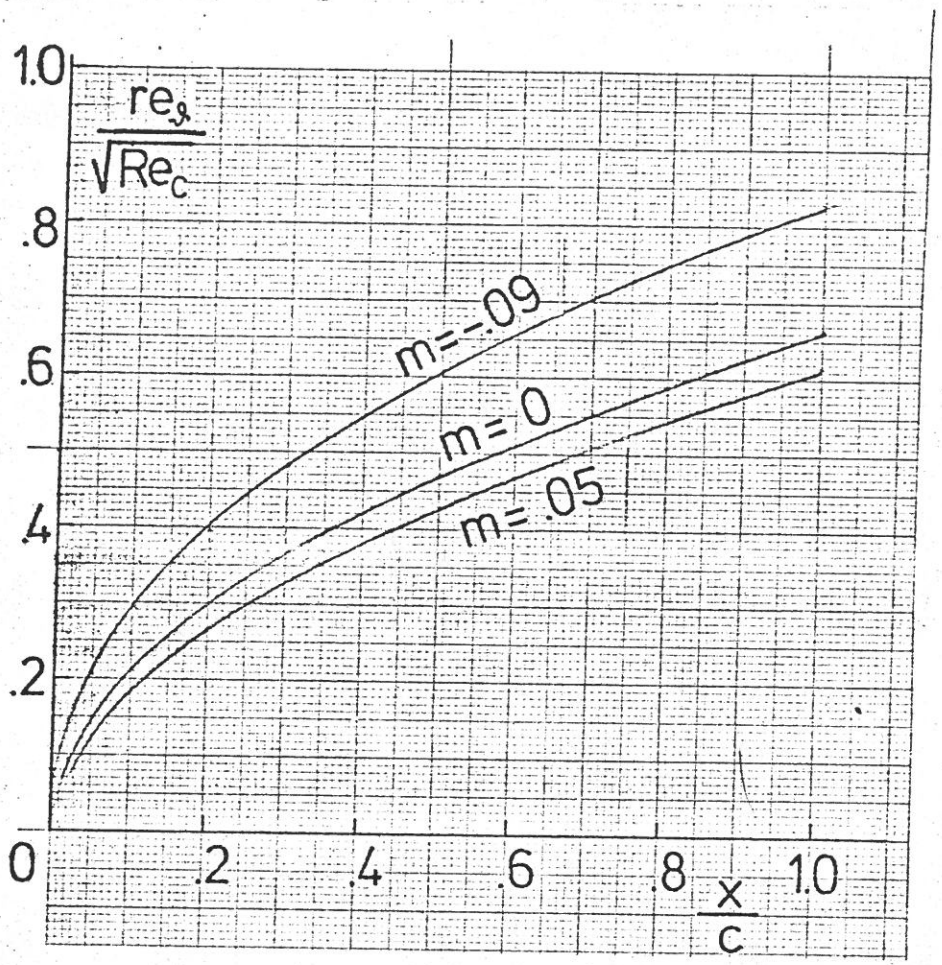

Fig.6 Laminar boundary layer thickness for some m-values

c) Separation bubble

Very often, especially at low Re_c-numbers, the laminar boundary layer will separate before it becomes turbulent. At high angles of incidence this happens at the airfoil nose even when the chord Reynoldsnumber is high, because the length Reynoldsnumber of the separation point is an order of magnitude lower.

Fig.7

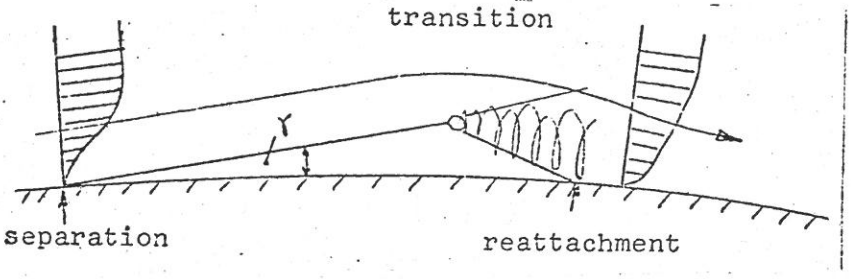

The separated boundary layer stays laminar for a while, leaving the wall in a nearly straight line. Downstream of the transition point the turbulent mixing is able to bend the average streamline towards the wall and to build up a certain pressure recovery up to the reattachment point (Fig.7).

Below the separating streamline the flow forms a closed region of dead air, the separation bubble. Fig.7 illustrates the situation and Fig.8 is a photographic side view of a bubble.

The pressure difference, which the turbulent mixing can realize, is restricted to values below say 35% of the dynamic head at the separation point - a situation similar to the Carnot shock in pipe flow with a discontinuity in area.

Fig.8

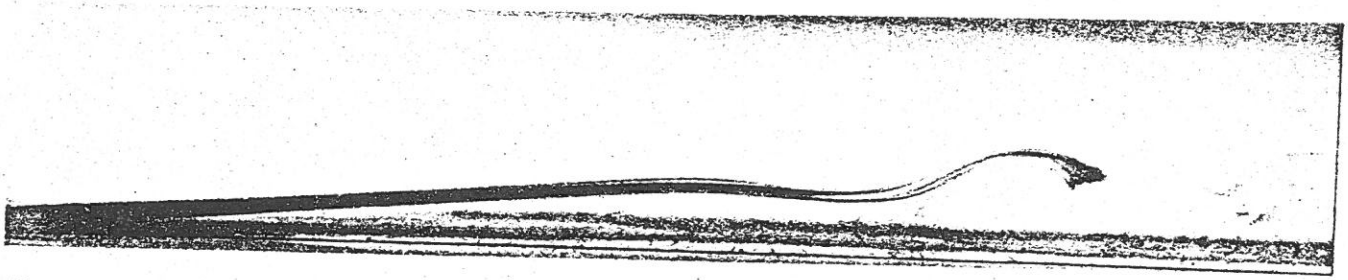

In the case of airfoils the final pressure recovery is equivalent to a certain streamline contour which in turn may be compatible with the geometric airfoil contour or not. Now the bubble behaviour can develop into two different types: the first occurs typically on thin and low cambered airfoils: with increasing angles of incidence the turbulent part of the bubble spreads out more or less along a line of constant pressure. The fluid contour on the

upper side resembles a cavitating bubble and redistributes the whole pressure distribution far away from the potential solution. The maximum lift will be reached when the bubble extends to the trailing edge.

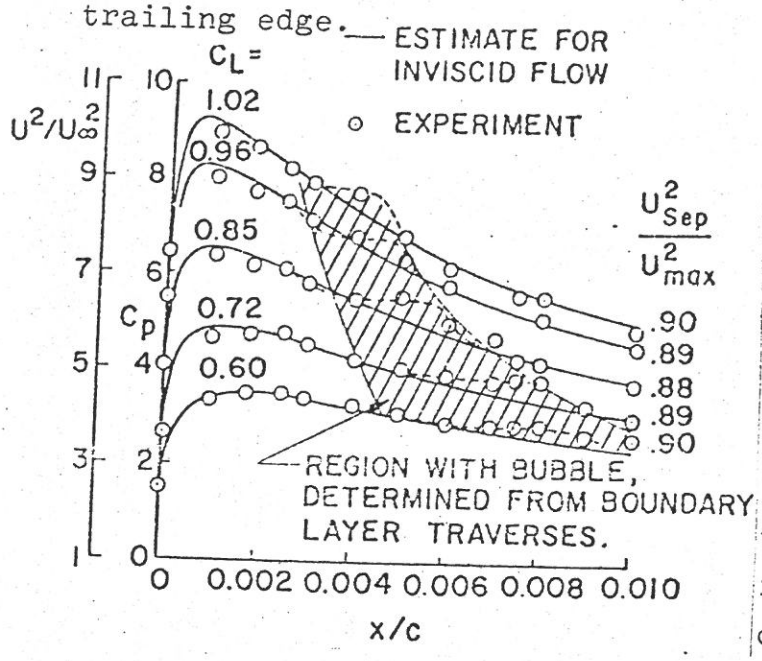

Fig.9

When the bubble is embedded in a softer overall pressure gradient and the curved streamline of the turbulent part of the bubble can meet the airfoil contour immediately, then the bubble looks like Fig.7 or 8: 80% of the bubble length are laminar and the rest turbulent. The effect on the overall pressure distribution is small as can be seen from Fig.9.

With increasing angles of incidence the bubble length reduces due to a faster transition downstream of the separation. The main reason for the quicker transition is the increasing wedge angle of the separation streamline. However, with higher incidences the overall pressure gradients become steeper and steeper and it is questionable whether the transition can be fast enough to avoid an unduly strong pressure recovery in the turbulent part of the bubble.

When this happens at high angles of incidence the tiny bubble suddenly explodes, but now there is no chance to reattach the surface in front of the trailing edge. There is no longer a closed bubble, only a completely separated flow.

Besides this dramatic effect on the stall of airfoils the separation bubble has a more subtle influence on the development of the following turbulent boundary layer.

The turbulent reattachment process constitutes an initial thickness for the turbulent boundary layer whose details are not very well understood. In any way we must be interested to hold this initial thickness as small as possible in order to avoid an unfavourable interaction with the following turbulent boundary layer.

The question whether the separation bubble harms the turbulent boundary layer or not may be answered by considering the turbulent boundary layer thickness at the reattachment point. If the wedge angle of the laminar separation is large any forward shift of the transition point due to say higher noise, roughness or Reynoldsnumber will reduce the initial thickness of the turbulent boundary layer. At small wedge angles of the bubble it is better not to shift the transition forward. Obviously, we have to compare the gradient of the turbulent momentum thickness $\frac{d\vartheta}{dx}$ or $\frac{d\delta^*}{dx}$ with the wedge angle of the separation bubble.

For the latter the author (7) found an approximate relationship

$$\tan\gamma = \frac{64\,\rho}{Re_{\vartheta_s}} \tag{12}$$

where $\rho = \frac{\vartheta_s^2}{\nu}\cdot\frac{dU}{dS}$ is a measure for the pressure gradient between the separation and reattachment point.

d) Turbulent boundary layer

If we exclude the possibility to maintain the laminar state by suction, the main pressure recovery in the rear part of an airfoil has to be done by the turbulent boundary layer. Today there exist many sophisticated methods to calculate the turbulent boundary layer, however, for our purposes a simple quadrature formula given by Truckenbrodt ( ) is good enough:

$$\frac{\vartheta}{c} = \left(\frac{U_\infty}{U}\right)^3\cdot\left[C + B\int_{x_1/c}^{x/c}\left(\frac{U}{U_\infty}\right)^{3.33} d\frac{x}{c}\right]^{.857} \tag{13}$$

with

$$C = \left[\left(\frac{U_1}{U_\infty}\right)^3\frac{\vartheta_1}{c}\right]^{1.166}$$

$$B = \frac{.0076}{Re_c^{.166}}$$

For the fully turbulent flat plate $x_1 = 0$ with $\frac{U_1}{U_\infty} = 1 = \text{const}$ and $C_1 = 0$ we get

$$\frac{\vartheta}{c} = \frac{.0152}{\left(\frac{U_1}{U_\infty}Re_c\right)^{.143}}\cdot\left(\frac{x}{c}\right)^{.857}$$

$$Re_\vartheta = .0152\left(\frac{x}{c}\cdot\frac{U_1}{U_\infty}\cdot Re_c\right)^{.857} \tag{14}$$

For the turbulent boundary layer we are interested in the following questions:

What is the influence of the pressure distribution and the initial values on the development of the boundary layer? Will the boundary layer separate? What is the influence of the Reynolds and Mach number? To begin with the last: for Mach numbers below one and adiabatic wall the influence on ϑ can be neglected. Only the displacement thickness is due to the heating somewhat larger than in incompressible flow and the separation occurs slightly earlier.

With respect to separation it is convenient to compare the kinetic energy at the start of the pressure rise to the rest of the flow. Before separation occurs, it is usually possible to recover 50% to 80% of the entry energy. Therefore it is reasonable to investigate boundary layers in terms of $(\frac{u}{u_1})^2$ or $(\frac{u}{u_1})$ and not $\frac{u}{u_\infty}$.

Fig.10 gives an example of the behaviour of turbulent boundary layers, taken from A.M.O.Smith (8). The type of pressure distribution and the initial values of the momentum thickness changes. It can be seen that all pressure distributions do not separate before $(\frac{u_e}{u_0})^2$ is less than .5. However, the concave distributions can realize a far greater pressure recovery especially when the initial boundary layer thickness is small.

In selecting suitable velocity distributions we are naturally interested into the special cases which produce the so-called "equilibrium" boundary layers. Such velocity distributions are concave all the way, starting with steep and ending with soft pressure gradients. Similar to the laminar counterpart a constant shape parameter is the trademark of such boundary layers. Also, the momentum and displacement thickness grow linearly with length. One extreme example, the turbulent boundary layer which comes everywhere close to separation, was investigated by Stratford (9).

Velocity distributions for equilibrium boundary layers can easily be calculated, depending on the initial values:

if U_1 is the velocity at the start x_1 of the pressure rise the concave velocity distribution may be described by

$$\frac{u}{u_1} = \left(1 + a\,\frac{x-x_1}{l-x_1}\right)^{-.24}$$

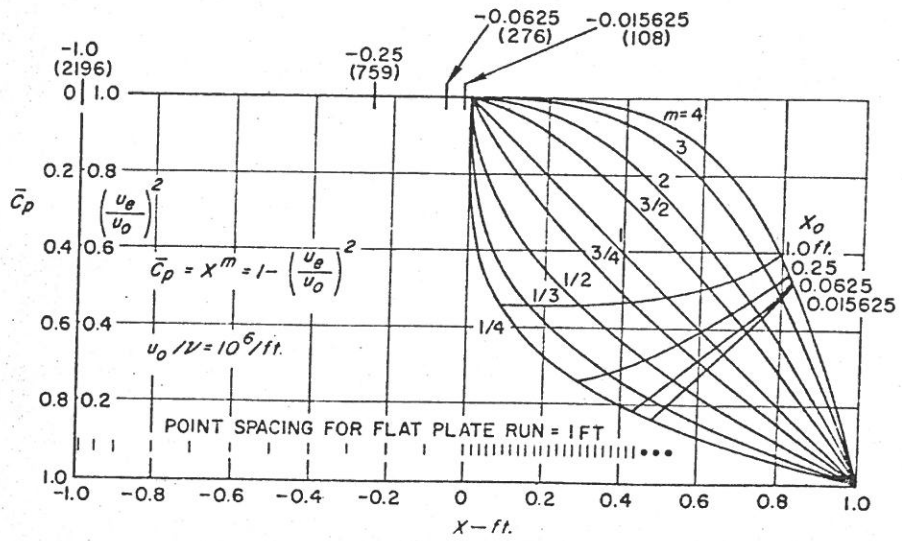

Fig.10 Separation of turbulent boundary layer as function of the pressure distribution and initial momentum thickness.

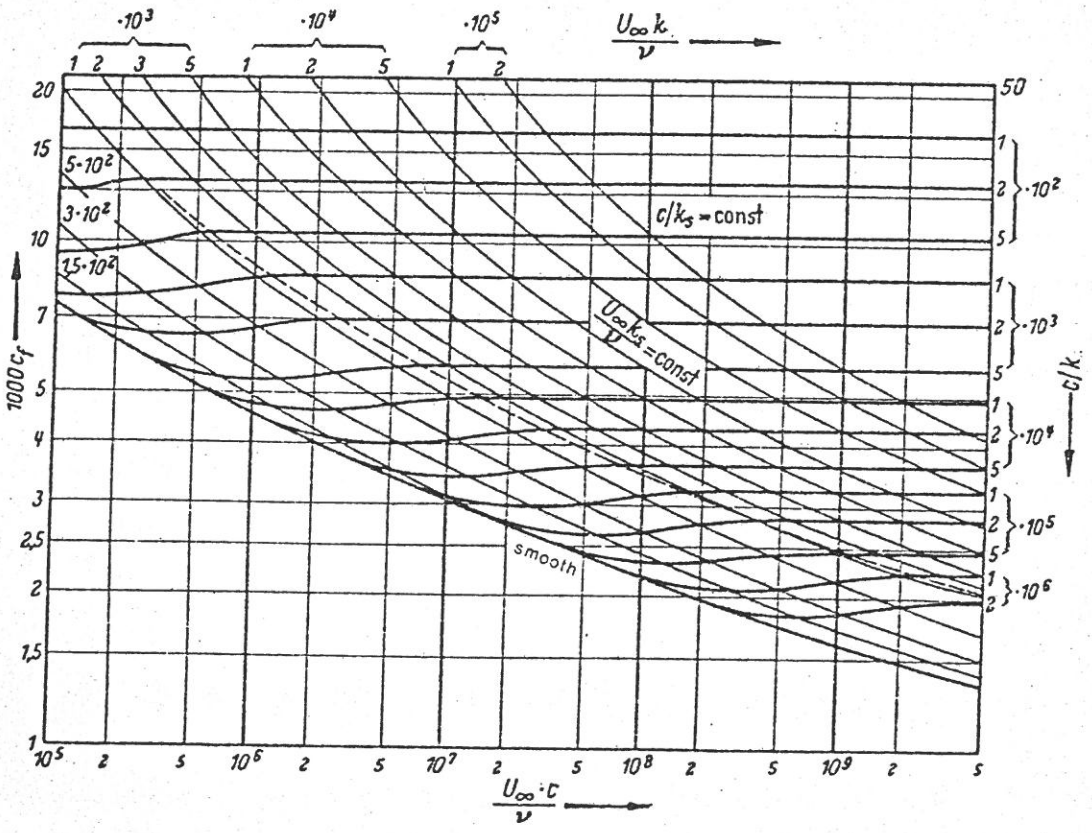

Fig.12 Skinfriction coefficient for smooth and rough plates

(15)

The constant a depends on the Reynoldsnumber of the turbulent part of the airfoil between x_1 and 1 at the trailing edge:

$$Re_1 = (1 - x_1)\, Re_c \cdot \frac{U_1}{U_\infty}$$

and the Reynoldsnumber of the initial momentum thickness (16)

$$Re_{\vartheta_1} = \frac{U_1 \vartheta_1}{\nu} = \frac{U_1}{U_\infty} \cdot \frac{\vartheta_1}{c} \cdot Re_c$$

and the shape parameter. Here the parameter H_{32} is used with $H_{32} = 1.732$ for the turbulent flat plate and 1.515 for separation. Fig.11 gives the connection to H_{12}.

Now for the factor a we can use

$$a \approx \frac{.012\, Re_1 (1 - 5 \cdot \Delta H_{32})}{Re_{\vartheta_1}} \qquad \Delta H_{32} = H_{32} - 1.575 \tag{17}$$

This simple formula gives a fast guess of the type and size of pressure rise which can be realized for a given initial condition and Reynoldsnumber. The thickness increase of ϑ is given by

$$\frac{\vartheta}{\vartheta_1} = 1 + a \left(\frac{x - x_1}{1 - x_1} \right) \tag{18}$$

Because the value of the constant a changes from the flat plate condition to separation by a factor of three, the last equation gives again a fast survey on the boundary layer development.

For the trailing edge we have

$$\vartheta(TE) = \vartheta_1 (1 + a) = \vartheta_1 \left(\frac{U_1}{U_{TE}} \right)^{4.166}$$

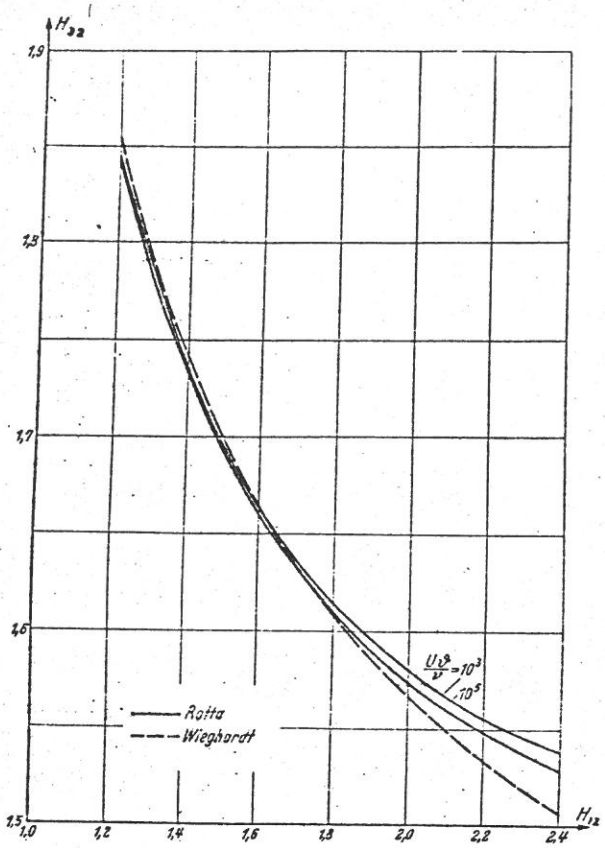

Fig.11 Relationship between H_{32} and H_{12} for turbulent boundary layers.

e) Longitudinal curvature

Because turbulent boundary layers are relatively thick they are sensitive to longitudinal curvature. A curved flow usually develops a quality which is not always recognized: the fluid is no longer homogeneous, but is stratified due to centrifugal forces. Only the potential vortex is an exception.

Boundary layer on walls convex to the mainflow are stable stratified like fresh water over salt water or heated gas over cold gas. The turbulent mixing has not only to work against viscosity but also against the stratification. Reducing the mixing means less impuls transport, less skin friction and a smaller $\frac{d\vartheta}{dx}$.

The boundary layer on convex walls behaves to a certain degree like a laminar boundary layer and will separate much earlier than a normal turbulent boundary layer. The contrary is true for the boundary layer on concave walls. The mixing is enhanced often with regular and counterrotating rolls (Taylor-Görtler vortices). On concave walls the separation is definitely delayed.

f) Roughness

Roughness can have a considerable influence on the drag of an airfoil. We have to distinguish between laminar and turbulent boundary layers. For turbulent boundary layers roughness will be felt, when the roughness height K becomes higher than the viscous sublayer. Therefore K has to be smaller than

$$\frac{v^+ \cdot K}{\nu} < 5 \qquad (19)$$

The friction velocity $v^+ = \sqrt{\frac{\tau_w}{\rho}}$ can be replaced by the local skin friction coefficient

$$v^+ = u_\infty \sqrt{\frac{c_f'}{2}}$$

with

$$c_f' = \frac{.059}{Re_x^{.2}} \qquad \text{for the flat plate.}$$

The roughness Reynoldsnumber has to stay below

$$\frac{u_e K}{\nu} < \frac{7}{\sqrt{c_f'}} \qquad (20)$$

Since c_f' changes only weakly with Reynoldsnumber we may write $R_x = R_c$ and get Table II

Re_c	$\frac{u_e K}{\nu}$
10^5	91
10^6	114
10^7	144
10^8	181

If we are interested in the small variation of the allowable roughness Equ.(20) may be written in the form

$$\frac{K}{c} \leq \frac{29}{Re_c^{.4}} \left(\frac{u}{u_\infty} \cdot \frac{x}{c}\right)^{.1} \qquad (21)$$

In the region of pressure rise the c_f'-value may be reduced to half the flat plate value.

An important question is how much does the drag increase if the roughness is larger than the allowable limit. If the values of TableII are doubled, then the drag will be about 20% higher.

If the roughness is five times larger, the additional drag will grow to

50 - 70% of the smooth value. Now the drag becomes independent of the Reynoldsnumber at all, see Fig.12. For a given value of $\frac{k}{c}$ the Reynoldsnumber is the most important factor, as can be seen for other $\frac{k}{c}$ in Fig.12. (Seite 10a)

In the laminar case, roughness plays a completely different role. Now roughness may shift the transition position. A two-dimensional roughness like a transition wire works primarily due to the small separation bubble it creates. In the reattachment region a much stronger amplification takes place than without the roughness. If the height of the roughness is plotted in terms of displacement thickness we observe a continuous changing transition position, see Fig.13. A rearward facing step in the contour has a very similar effect. For three-dimensional roughness the behaviour is slightly different. Up to a ratio of $\frac{k}{\delta^*} < .5$ the transition will not be influenced. For higher roughness the transition jumps immediately to the roughness position.

Small surface waves are not important in regions with strong favourable pressure gradients. For flat plate conditions a single wave will also destabilize the laminar boundary layer.

A stronger effect has a sequence of waves, because the boundary layer develops a memory for the waves and dependent on the wave amplitude will separate after 5 - 8 waves, even when the amplitude is as low as $\frac{k}{\delta^*} < .15$.

If we compare the roughness height, which will not shift the transition and not increase the turbulent skin friction we find for higher Reynoldsnumbers that the turbulent boundary layer requires usually a smoother surface than the laminar flow, see Fig.14. It should be mentioned that leakages are also a sort of roughness.

Sometimes it is of interest to provoke transition. Three-dimensional roughness with supercritical height along a small strip may do it. For low Reynoldsnumbers a three-dimensional roughness of special form (see Fig.15) may be more effective than other types of roughness. The height of the forward facing step may be K. Then a Reynoldsnumber

$$\frac{4k}{\nu} \geq 120 \div 150$$

seems to be necessary.

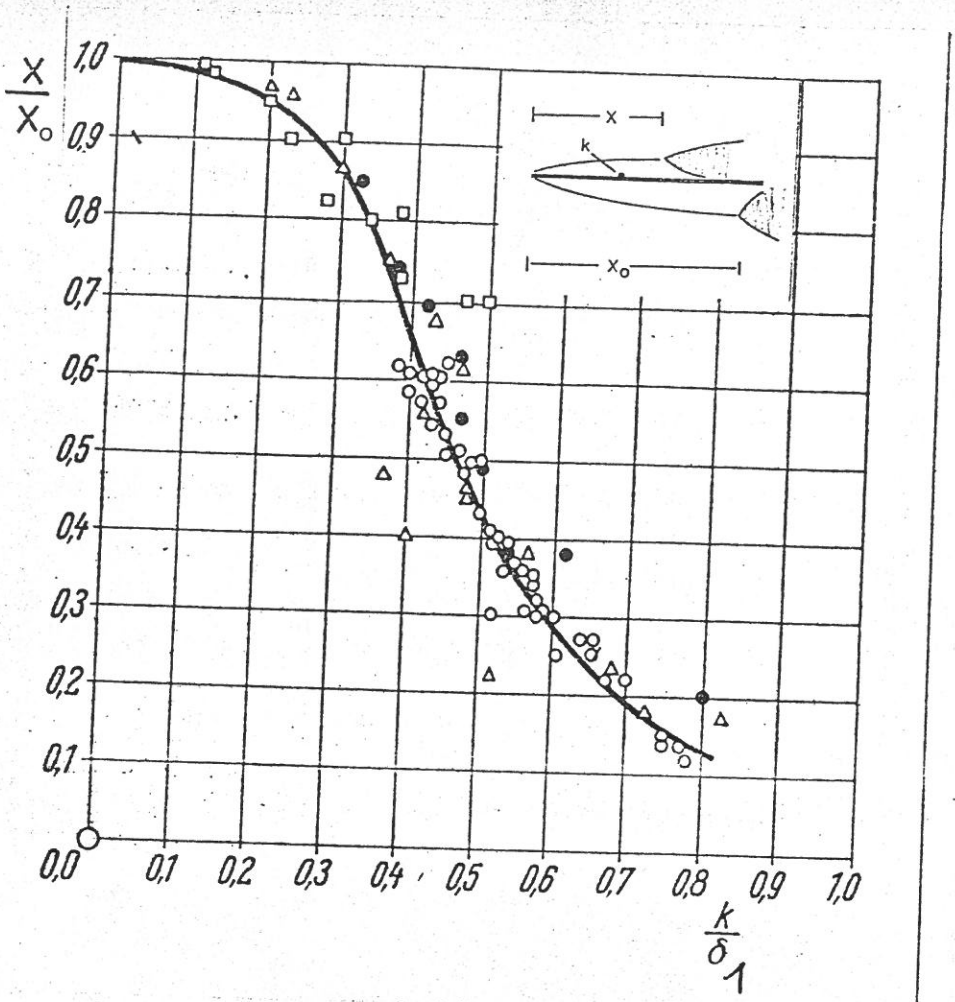

Fig.13 Influence of twodimensional roughness on transition

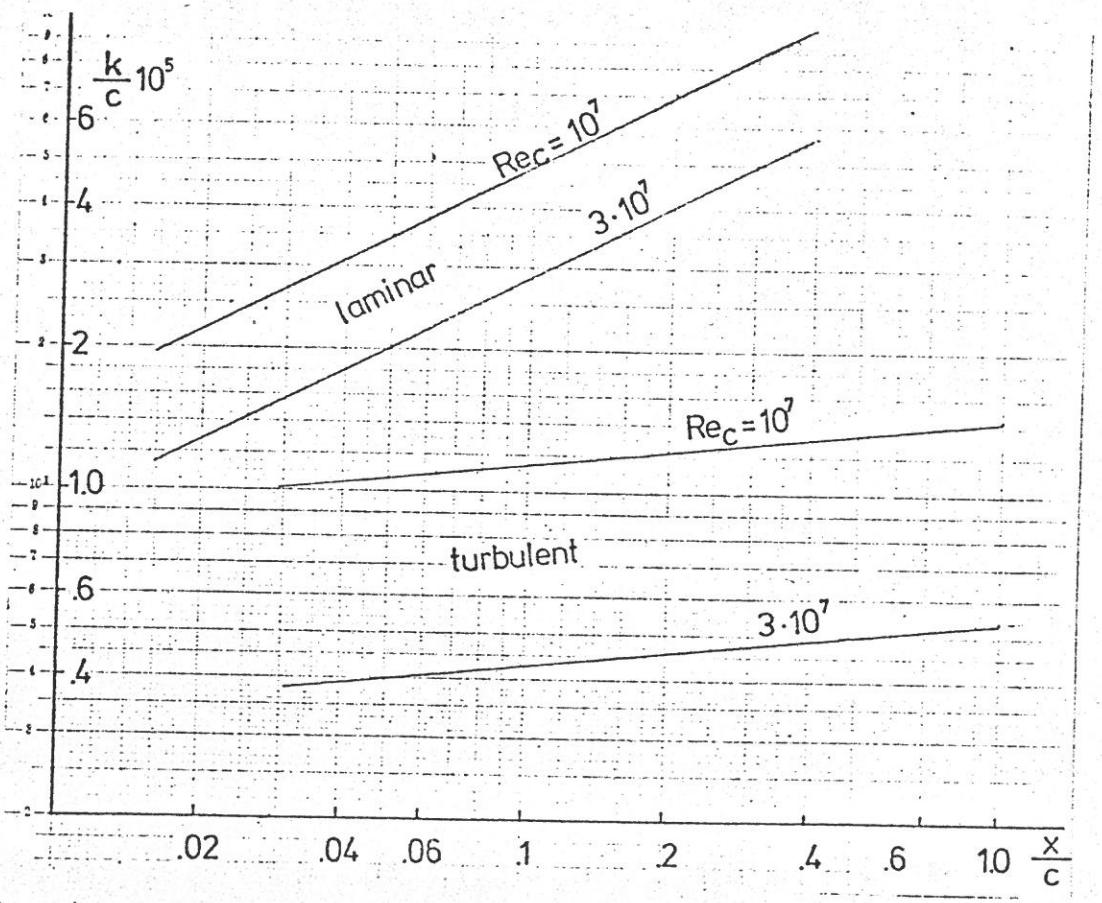

Fig.14 Critical roughness for a flat plate at two Reynolds-numbers for the laminar and turbulent boundary layer

The oncoming flow is divided into single streaks which provoke double vortices in the shearlayer which are followed by small local separations. The spanwise wave length of this device seems not to be critical.

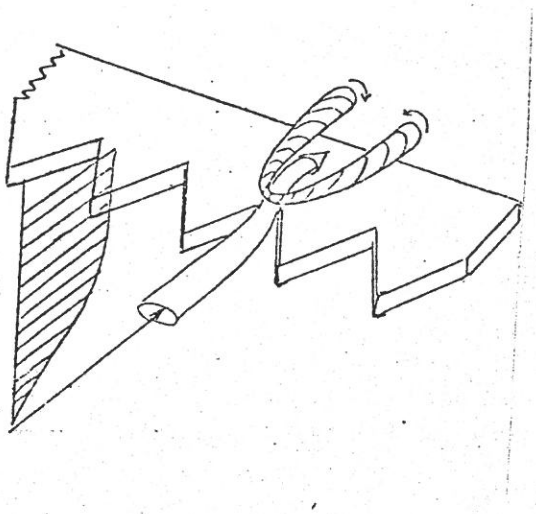

Fig.15 Threedimensional roughness to trigger transition

II. Potential flow over single element airfoils

In this chapter we will learn about the connection between the pressure distribution and the shape of the airfoil and the implied constraints. In order not to ask the computer any time it is helpful to have a rough survey on typical qualities of airfoils. In the following we will separate these qualities on the basis of potential flow.

a) Symmetrical airfoils at zero angle of incidence

The most simple airfoil in a theoretical sense is the elliptical airfoil. If we denote the related coordinates and velocities

$$\frac{x}{c} = X$$

$$\frac{y}{c} = Y \qquad \frac{2 \cdot y_{max}}{c} = \delta \quad \text{airfoil thickness}$$

$$\frac{u}{u_\infty} = U$$

and $$X = \frac{1}{2}(1 + \cos\varphi) \tag{22}$$

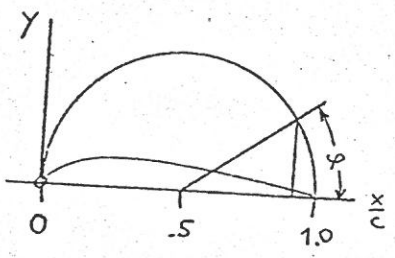

Fig.16

where φ is a circular angle, defined as in Fig.16, then the shape of the ellipse is given by

$$Y = \delta \sqrt{X(1-X)} = \frac{\delta}{2}\sin\varphi$$

The velocity distribution comes as

$$U = \frac{1+\delta}{\sqrt{1 + (\delta \cdot \operatorname{cotan}\varphi)^2}} = 2(1+\delta)\sqrt{\frac{X(1-X)}{1-(1-\delta^2)(1-2X)^2}}$$

and

$$U_{max} = 1 + \delta$$

There are two extremes of the elliptical airfoil: the circular cylinder with $\delta = 1$ and the flat plate with $\delta = 0$. Fig.17 shows the velocity distribution of several elliptical airfoils. The supervelocity due to the thickness depends immediately on δ, the relative thickness. Near the ends $x = 0;\ \varphi = 0$
$x = 1;\ \varphi = \pi$
the values of cotanφ become large against 1, therefore the velocity gradient can be approximated by

$$\frac{dU}{d\varphi} \approx \frac{1+\delta}{\delta} \tan\varphi \qquad \lim_{\substack{\varphi \to 0 \\ \varphi \to \pi}} \tan\varphi = 1$$

Another simple airfoil is the linearized Joukowsky airfoil. The shape and velocity are given by

$$y = 2\varepsilon\sqrt{x(1-x)^3} = \frac{\varepsilon}{2}\sin\varphi\,(1-\cos\varphi)$$

$$\varepsilon = .77\,\delta$$

$$U = \frac{1+\varepsilon(1-2\cos\varphi)}{\sqrt{1+\varepsilon^2\left(\frac{\cos\varphi-\cos^2\varphi}{\sin\varphi}\right)^2}}$$

Both the maximum thickness and the maximum velocity are shifted forward to x = .25 and x = .15 respectively. Joukowsky airfoils have a cusped tail and zero trailing edge angle yielding a final trailing edge velocity $U_{TE} = 1 - \varepsilon = 1 - .77\delta$. Fig.18 shows the velocity distributions for some δ-values.

The well-known NACA thickness distribution of the four- and five-digit airfoils is given by

$$y = 2.5\cdot\delta\,(.2969\sqrt{x} - .126x - .3516x^2 + .2843x^3 - .1015x^4)$$

The maximum thickness lies at x = .30.
A number of velocity distributions is given in Fig.19.

The velocity distributions of the NACA-6 series airfoils for different positions of the maximum velocity and for $\delta = .12$ are given in Fig.20.

With respect to the velocity gradient at the nose all airfoils exhibit an increasing gradient with decreasing thickness. The contrary is true for the trailing edge velocity gradient (with the exception of the blunt elliptical airfoils).

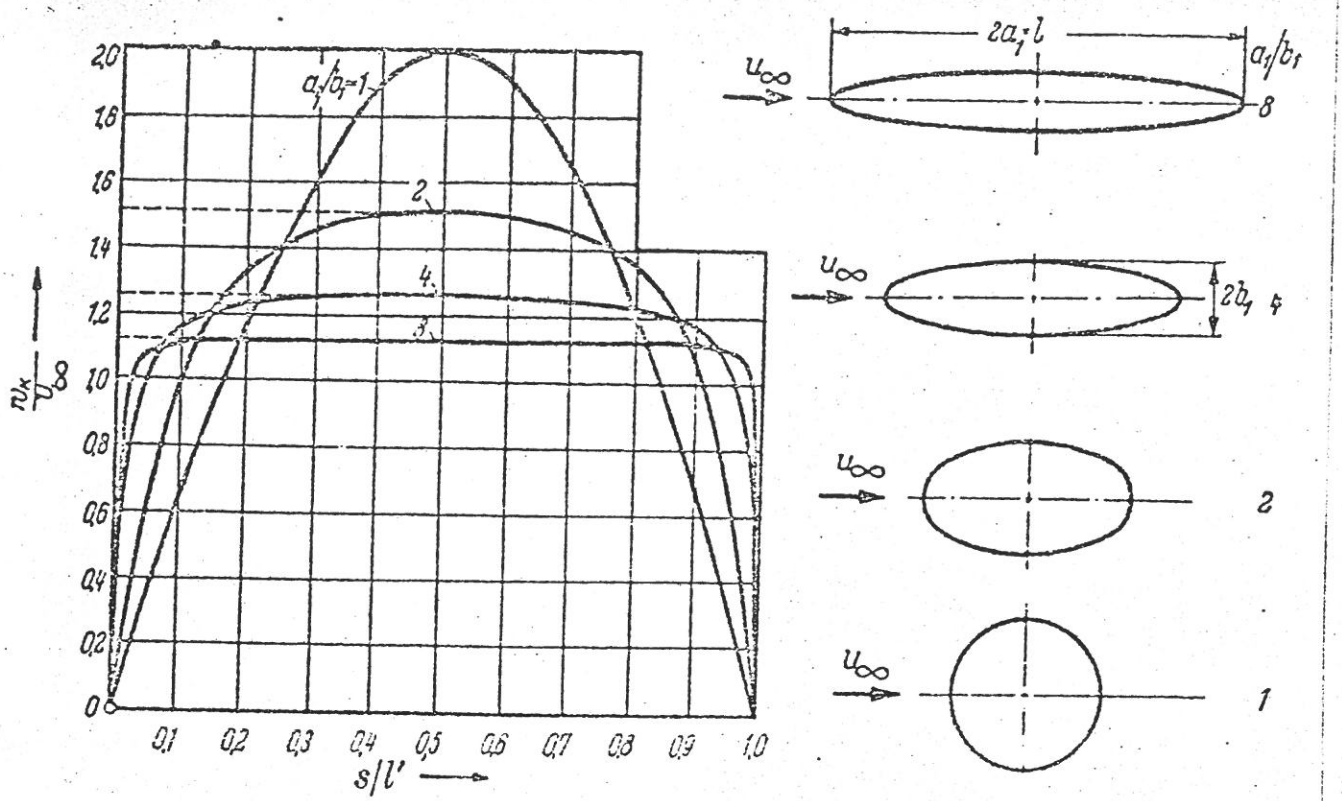

Fig.17 Velocity distribution of several elliptical airfoils

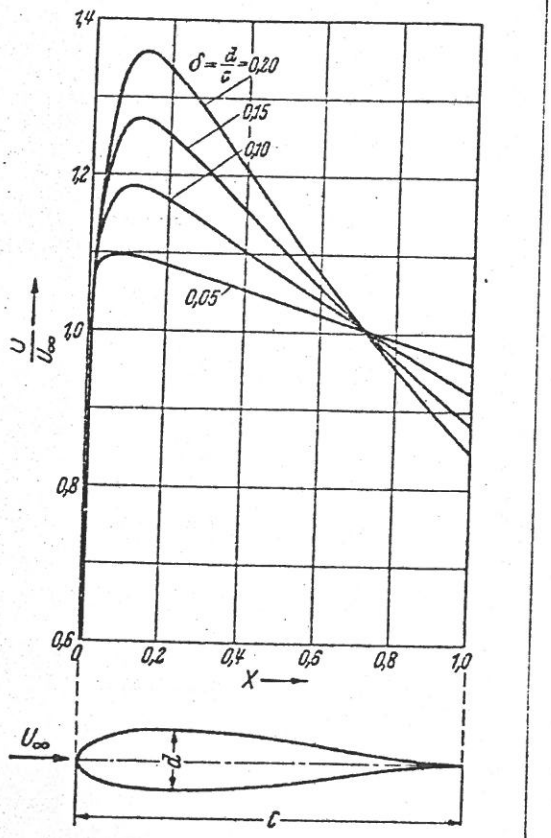

Fig.18 Velocity distribution of several Joukowsky airfoils

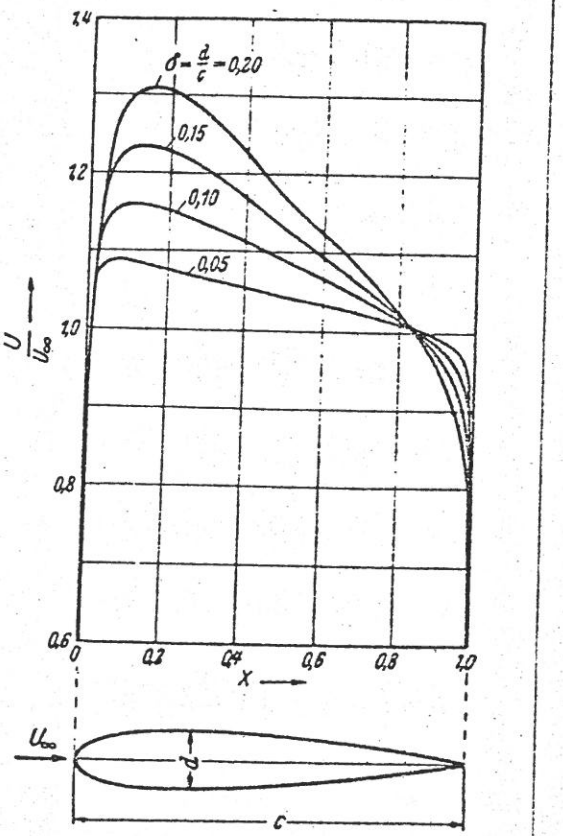

Fig.19 Velocity distribution of several NACA OOXX airfoils

Fig.21 illustrates the velocity gradients at the nose for the Joukowsky airfoils and gives also some values of the elliptic and the NACA-6 airfoils.

In Fig.22 the maximum supervelocity of these different airfoils is shown as function of the relative thickness δ . Again it can be seen that the Joukowsky airfoils, with a maximum thickness position at x = ,25 , and the elliptic airfoil with δ_{max} at midchord encompass other more practical airfoils.

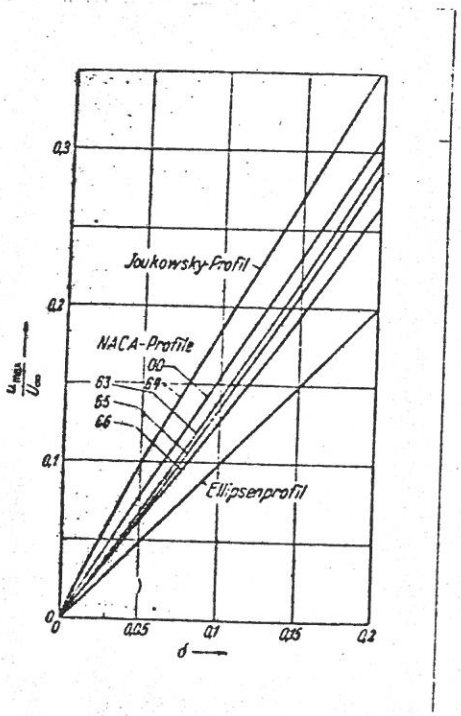

Fig.22 Supervelocity of several airfoil clases

b) Angle of Incidence

Airfoils with sharp trailing edge usually satisfy the so-called Kutta-Joukowsky condition which means a smooth trailing-edge flow. Then any deviation from the zero lift angle produces a circulation and hence lift. The same is true for airfoils with blunt trailing edges, when the rear stagnation point is fixed. For elliptical airfoils the change in lift coefficient is

$$\frac{dc_L}{d\alpha} = 2\pi(1+\delta)$$

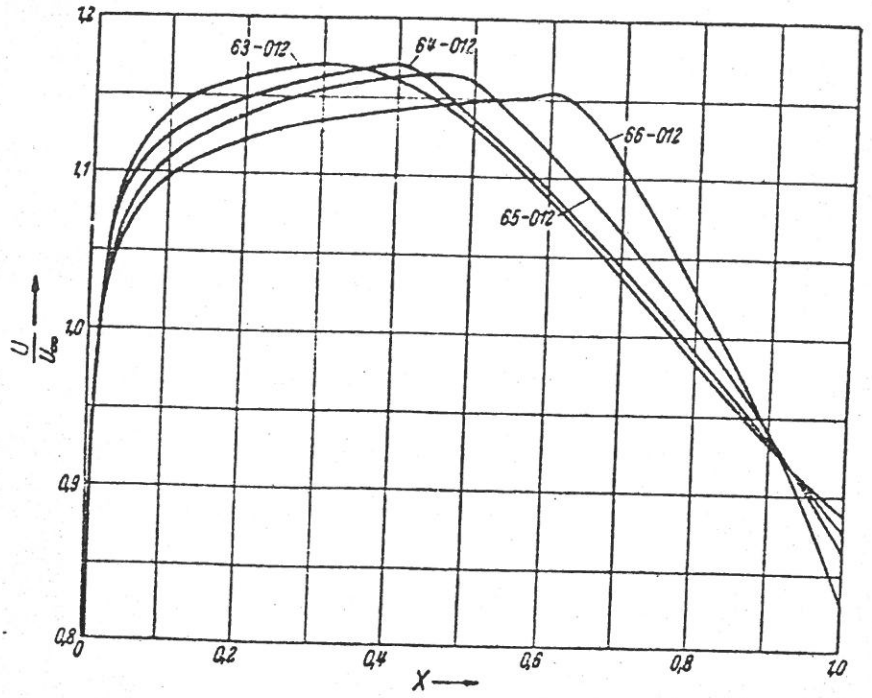

Fig.20 Velocity distribution of several NACA 6X-012 airfoils

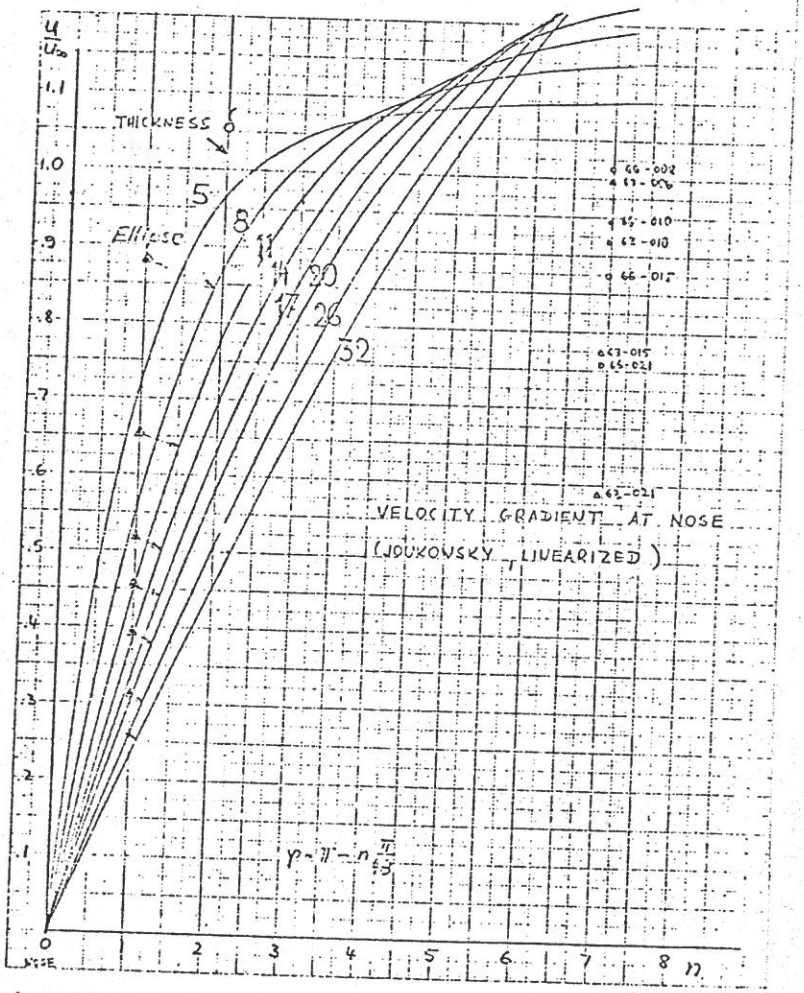

Fig.21 Velocity gradients near the nose of Joukowsky airfoils

(28)

i.e. 2π for the flat plate and 4π for the circualr cylinder.

For Joukowsky airfoils we have

$$\frac{dc_L}{d\alpha} = (1 + .77\delta)\, 2\pi \tag{29}$$

In viscous flow the increase of $\frac{dc_L}{d\alpha}$ due to thickness is practically cancelled by the thicker boundary layers of these airfoils. For fully turbulent flow and for $\delta \approx .2$ $\frac{dc_L}{d\alpha}$ may be even 5% less than with thin airfoils. Generally in real flow a cusped trailing edge satisfies the Kutta-Joukowsky conditions better than a wedge shaped.

The pressure distribution due to the angle of incidence for a flat plate is

$$u = \cos\alpha \pm \sin\alpha \sqrt{\frac{1-x}{x}} \qquad + = \text{upper side}$$

$$\text{or} \qquad \Delta u = 2\sin\alpha \sqrt{\frac{1-x}{x}} \qquad - = \text{lower side} \tag{30}$$

yielding a pressure difference of

$$\frac{\Delta p}{q_\infty} = \Delta c_p = 2\sin 2\alpha \sqrt{\frac{1-x}{x}} \tag{31}$$

which by integration leads to $c_L = 2\pi \sin\alpha$.

Fig.23 shows the function $\sqrt{\frac{1-x}{x}}$. The center of lift acts on the point $x = .25$. The stagnation point on the lower side is shifted to $\sin^2\alpha$. This type of pressure distribution is typical for all thin airfoils with fixed trailing edge conditions. However, the well rounded nose shape of real airfoils reduces the flow velocities there to finite values.

For elliptical airfoils the more general velocity distribution is given by

$$u = \frac{1+\delta}{\sqrt{1 + (\delta \cot\varphi)^2}} \left(\cos\alpha \pm \sin\alpha \sqrt{\frac{1-x}{x}}\right) \tag{32}$$

If we compare this equation with the flat plate formula we see the role of the square root: for $\varphi \to \pi$ $\cot\varphi$ goes to infinity and makes the velocity now finite. Incidentally $\delta \cot\varphi$ has a geometric interpretation: it is the slope of the airfoil contour.

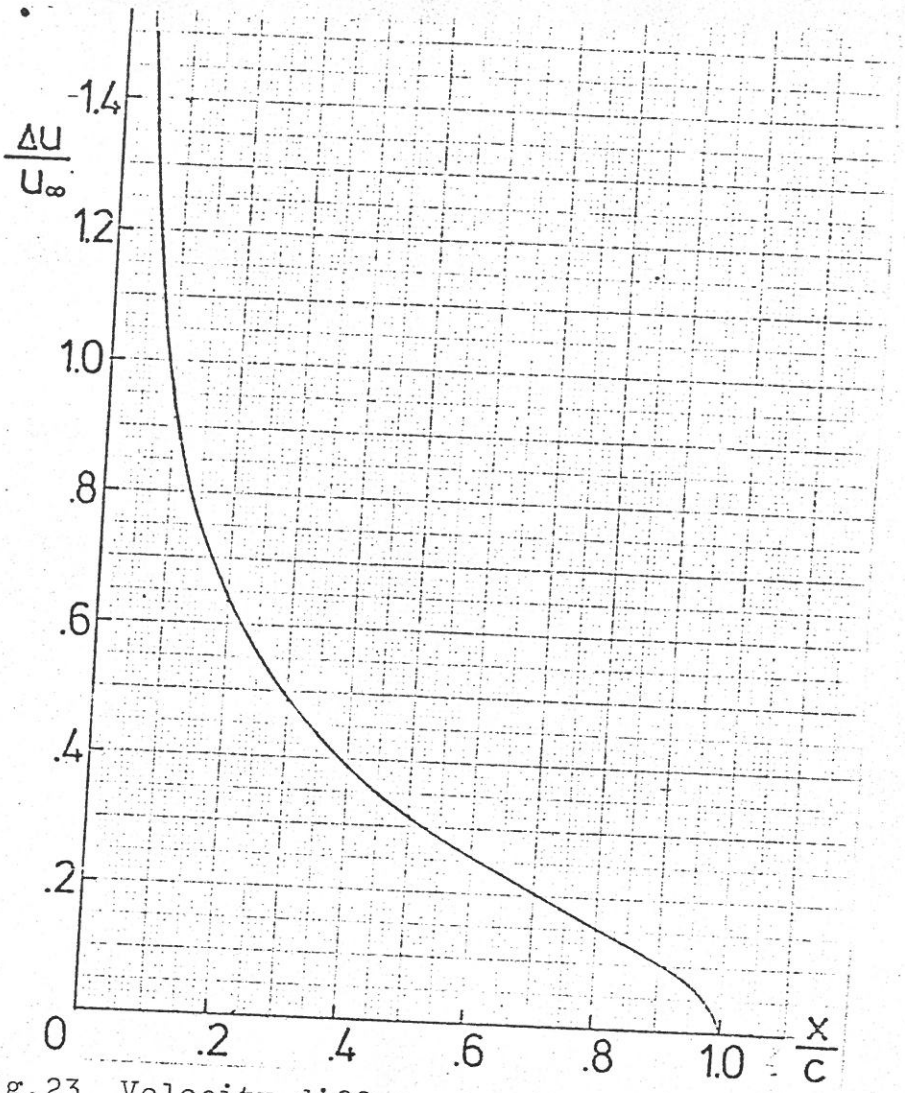

Fig.23 Velocity difference of flat plate at $2 \cdot \sin\alpha = 1/\pi$ or $c_l = 1.0$

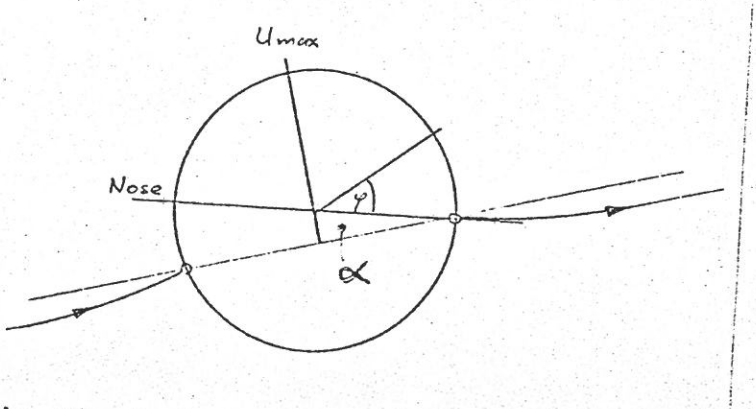

Fig.24 Potential flow around a circular cylinder with circulation

At the nose, where $\varphi = \pi$, the ratio $\frac{\infty}{\infty}$ reduces to

$$u(\pi) = \frac{1+\delta}{\delta} \cdot 2 \sin\alpha \tag{33}$$

If we connect the lift coefficient

$$c_L = 2\pi(1+\delta)\sin\alpha$$

and the nose radius ϱ of the ellipse with the thickness δ

$$\delta = \sqrt{2\varrho}$$

we have

$$u(\pi) = \frac{c_L}{\pi\delta} = \frac{c_L}{\pi\sqrt{2\varrho}} \tag{34}$$

In contrast to the flat plate, the nose velocity is not the peak of the velocity distribution, except at $\alpha = 90^\circ$. This can easily be seen in the following way: the circular cylinder with circulation, see Fig.24, has the maximum velocity at $\varphi = \frac{\pi}{2} + \alpha$. Since the velocity is

$$u(\alpha,\varphi) = 2\left[\sin(\varphi-\alpha) + \sin\alpha\right] \tag{35}$$

the maximum velocity is

$$u_{max}(\alpha) = 2\left[1 + \sin\alpha\right]$$

and the nose velocity at $\varphi = \pi$

$$u(\pi) = 4\sin\alpha$$

Only for $\alpha = 90^\circ$ the maximum velocity coincides with the nose and this holds for any airfoil, because airfoils work only for low angles of incidence, say 15 degrees; the nose radius therefore is not as significant as is often believed.

It is the shape of the whole nose region which is important for the type of velocity distribution at such angles of incidence.

In order to have a simple access to the influence of the angle of incidence, we may take Equ.(35) and formulate the ratio of velocities at two different angles of incidence, say α_1 and α_2 +)

$$\frac{u(\alpha_1,\varphi)}{u(\alpha_2,\varphi)} = \frac{\sin(\varphi-\alpha_1)+\sin\alpha_1}{\sin(\varphi-\alpha_2)+\sin\alpha_2} = \frac{\cos(\frac{\varphi}{2}-\alpha_1)}{\cos(\frac{\varphi}{2}-\alpha_2)} \tag{36}$$

+) In these equations α is always counted from the zero lift direction.

If one velocity distribution is known, say for α_1, the other for α_2 follows immediately. Since the velocity ratio is invariant against transformations like conformal mapping, the ratio holds for all airfoils if we know the relationship between a point of the airfoil contour and the associated φ-value on the circular cylinder. Equ.(22) is exact for elliptical airfoils and a good approximation for all other airfoils with nearly elliptical nose except for the first few percent of the chord.

c) The influence of camber
on velocity distribution and drag

The singularity method understands the velocity distribution of a cambered airfoil as composed by the thickness and a camber distribution and the effect of angle of incidence. This implies a definition of the latter, which takes the chord of the mean line as reference.

Now the purpose of the camber is to produce lift without angle of incidence due to velocity differences on the upper and lower sides of the airfoil. On symmetrical airfoils the effects of the angle of incidence can partly be influenced by the thickness distribution. Camber however gives a large degree of freedom to change the velocity distribution on both sides of an airfoil and partly independent of each other.

One of the simplest conceivable types of velocity differences is the constant difference at $\alpha = 0^\circ$ (NACA meanline with a = 1.0). If U_S is the velocity of an symmetrical airfoil and ΔU the total and constant difference between velocities on both sides then U can be composed by

$$U = U_S \pm \frac{\Delta U}{2}$$

and

$$c_p = \frac{U_u^2 - U_L^2}{U_\infty^2} = 2\left(\frac{\Delta U}{U_\infty}\right)\left(\frac{U_S}{U_\infty}\right) \tag{37}$$

and

$$c_L = \int_0^1 \Delta c_p \, dx \approx 2\left(\frac{\Delta U}{U_\infty}\right) \quad \text{for thin airfoils with } \frac{U_S}{U_\infty} \approx 1 \tag{38}$$

For other ΔU-distributions the mean value $\overline{\Delta U} = \int_0^1 \Delta U \, dx$ can give an approximation for the lift coefficient.

The NACA meanline (Fig.26, a = 1,0) has the contour

$$y = -\frac{c_L}{4\pi}\left[(1-x)\ln(1-x) + x \ln x\right] \qquad (39)$$

$$y(0.5) = \frac{c_L}{2\pi} \cdot .3465 = 5.516 \cdot 10^{-2} \cdot c_L = y_{max}$$

This type of meanline was introduced in connenction with the NACA 6 laminar airfoils (10), because it does not change the velocity gradients of a symmetrical airfoil. Therefore the qualities of symmetrical airfoils can be transferred more or less unchanged to cambered airfoils.

The lift of the constant loading at $\alpha = 0^o$ centers at the mid-chord point. Any other angle of incidence produces an additional lift which centers at the quarter chordpoint. The combined overall lift therefore shifts fore and aft between these points with the angle of incidence.

Sometimes as with helicopter rotors the pitching moment has to be nearly zero. Then this type of camber can not be applied. The rear part of the airfoil has to be unloaded or even downloaded and the front part has to carry more lift, so the center of the lift stays near the quarter chord point.

It is unavoidable that now for a given lift coefficient the supervelocities go up, see Fig.25.

For higher Mach numbers the supervelocity should be as small as possible. This can be achieved by loading the rear part of the airfoil, where supervelocities due to the thickness diminish. Now the front part is unloaded leading to the somewhat strange appearance of the modern transonic airfoils. The large pitching moments and the associated trim drag of these airfoils partly cancel their advantages.

Fig.25 shows how the lift loading can be varied from low to large pitching moments. (11)

For viscous flow the large velocity differences at the trailing edge are not possible. The boundary layer displacement thickness which is different on the upper and lower side changes the effective meanline, which changes the pressure distribution and this in turn the boundary layer. Therefore it is not possible to increase the lift simply by higher and higher cambered meanlines

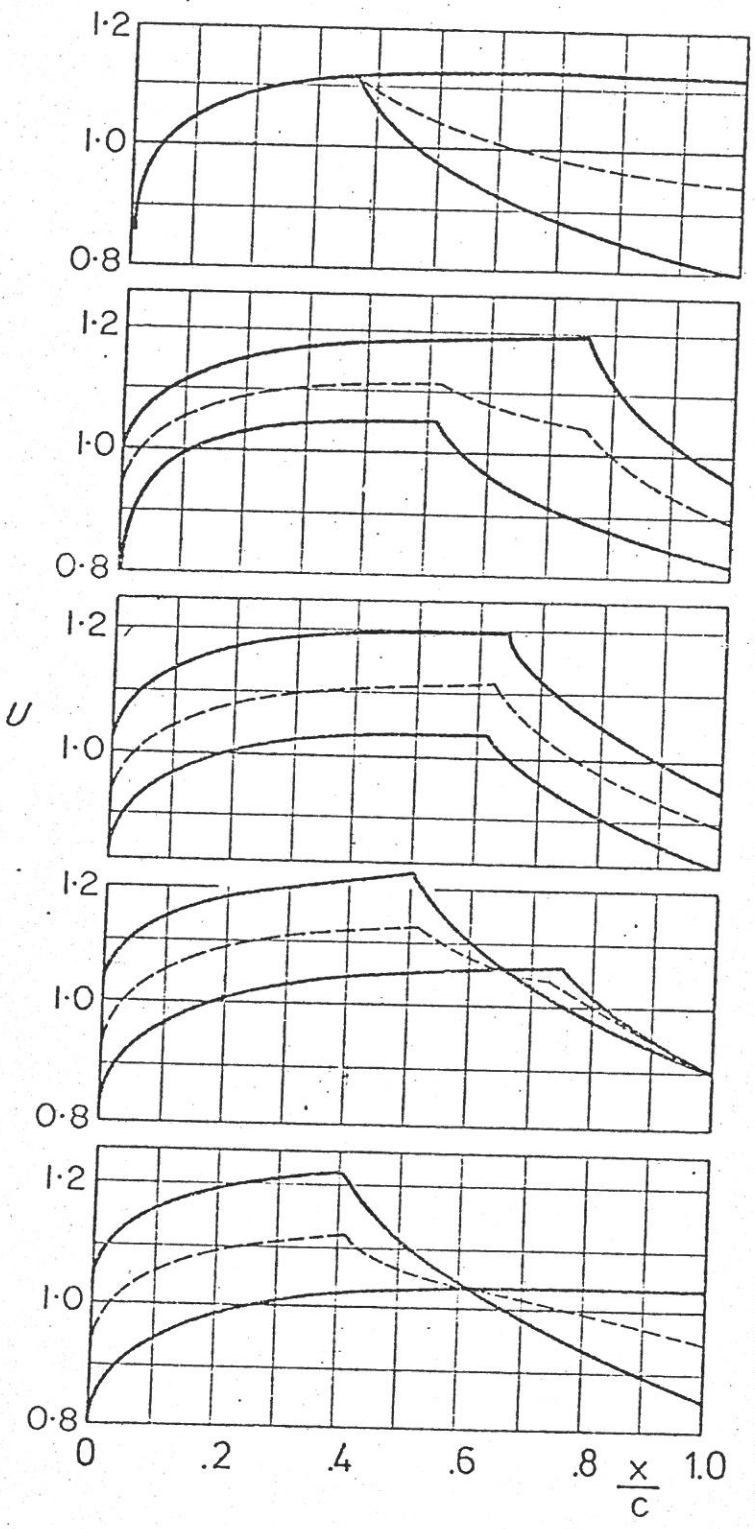

Fig.25 Systematic variation of the lift distribution

of the NACA a = 1.0 type. (See also the section on turbulent boundary layers.) Some experience seems to indicate that unseparated flow is not possible when the camber of the upper surface itself exceeds 15-17%. However, if drag doesn't matter, even high cambered meanlines up to 25% may be sensible for high lift production.

Fig.26 compares the NACA meanlines at a $C_L = 1{,}0$ for four different a-values.

d) Flaps

Here I would like to restrict myself to the simple plainflaps as one of the most convenient ways to change the geometry of an airfoil in order to produce control forces. The availability of variable geometry adds another degree of freedom to the design or selection of airfoils.

The simplest airfoil with a flap is a flat plate with a kink. If we denote the connection between the endpoints as chord and the difference between freestream and chord α (see Fig.27), as angle of incidence, then with

$$t = \sqrt{\frac{1-x}{x}}$$

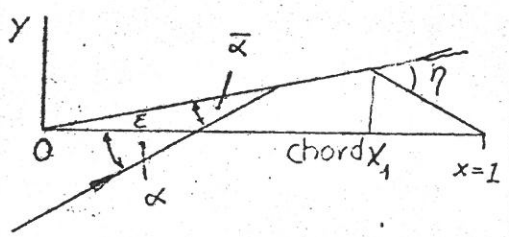

Fig.27

η as flap angle and $(1-x_1)$ as flap chord and $\varepsilon \approx (1-x_1)\eta$

the velocity distribution (see (12)) becomes

$$u \approx \left[1 - \frac{\tan\eta}{\pi}\left(2\ln\left|\frac{t_1 - t}{t_1 + t}\right| + \pi t(1-x_1) - t\varphi_1\right)\right]\cos\alpha + t\sin\alpha \qquad (40)$$

For a certain angle of incidence α_i the flow at x = 0 will be tangential to the airfoil:

$$\bar{\alpha}_i \approx \eta\left[(1-x_1) - \frac{\varphi_1}{\pi}\right] \qquad \varphi_1 = \arccos(2x_1 - 1) \qquad (41)$$

For $x_1 = .5$ we have a special type of meanline, symmetrical around the midchord point. For such meanlines α_i is always zero. For $x_1 > .5$ α_i is negative. The ratio of α_i to the flap angle η is given in Fig.28. The corresponding velocity distribution

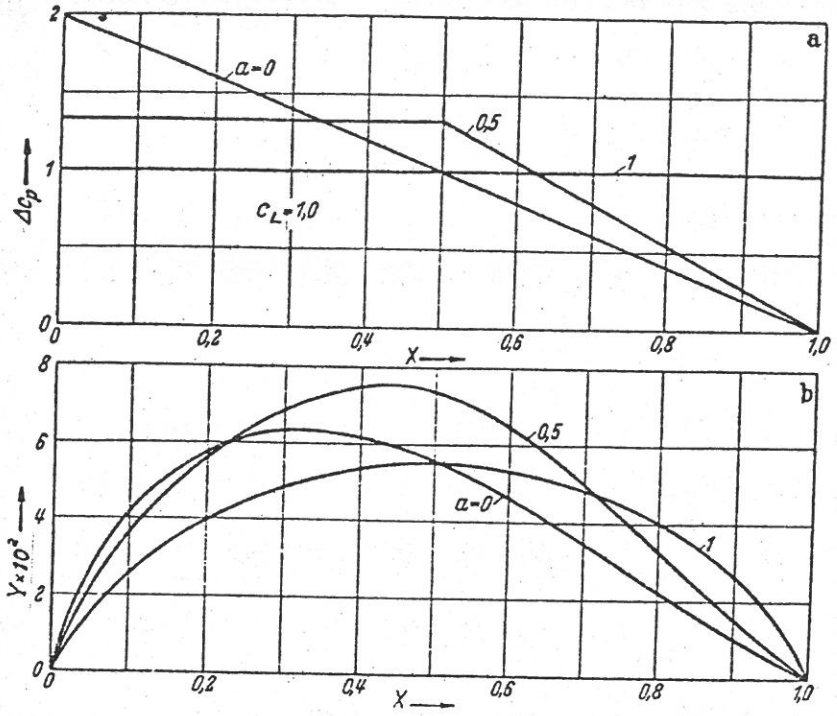

Fig.26
Three typical NACA meanlines and pressure distribution for c_L = 1.0

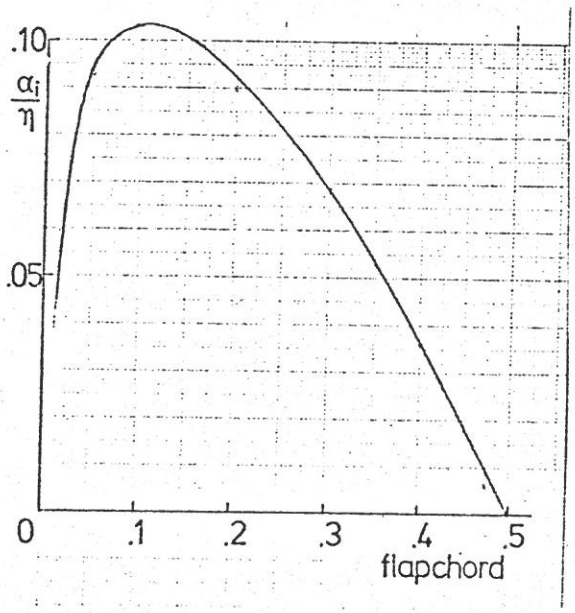

Fig.28
Ratio of the ideal angle of incidence α_i to the flap angle η

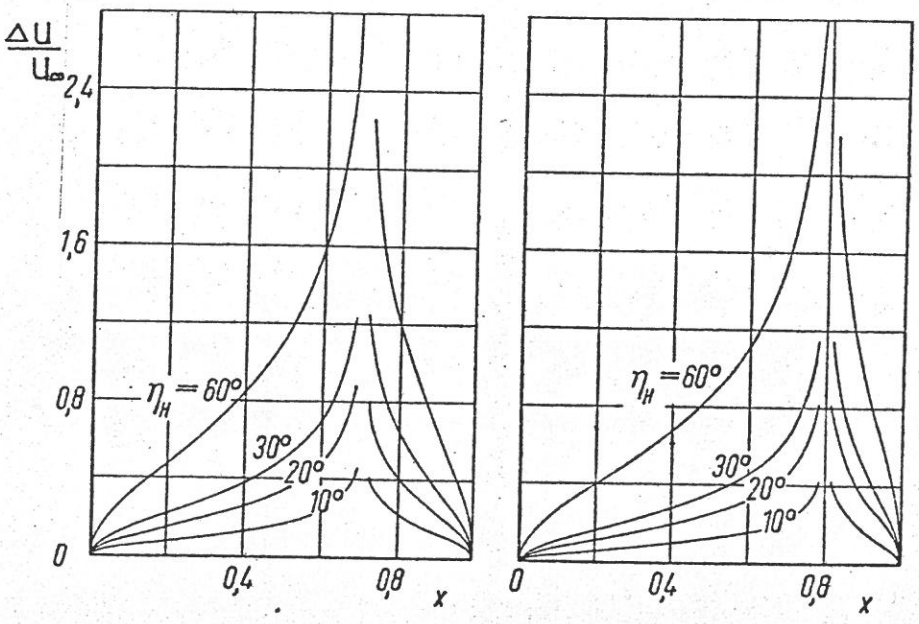

Fig.29
Lift distribution for flat plate with flap angle and $\alpha = \alpha_i$ for a flap chord of .2 and .3

is given in Fig.29 for $x_1 = .7$ and $x_1 = .8$ and several η-values. If we change the angle of incidence to $\alpha = \varepsilon$ the freestream has the same direction as the front part of the flat plate. The velocity distributions are given by Fig.30 and the c_L-values for some x_1 and flap angles in Fig.31.

It is not difficult to imagine that for small flap angles and angles of incidence between α_i and $\alpha = \varepsilon$ it should be possible to produce a more or less constant velocity distribution in front of the kink. With the help of a suitable thickness distribution this is certainly attainable. This opens the possibility to design a symmetrical airfoil with a deflected flap and to have at the same time favorable pressure distributions for the boundary layer control.

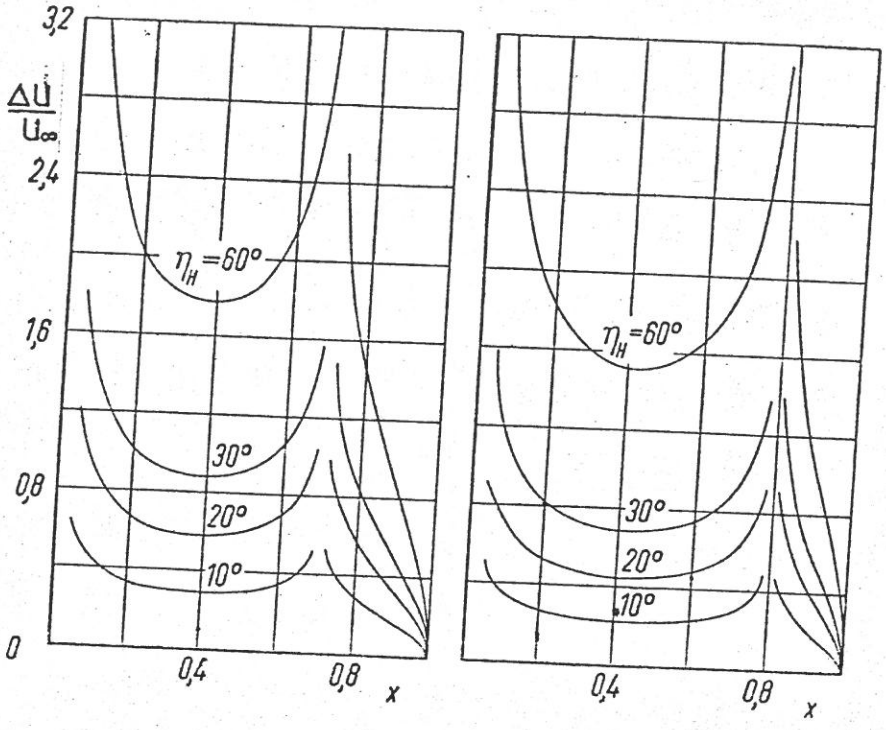

Fig.30 Lift distribution for $\alpha = \varepsilon$ on a flat plate with flap at $x_1 = .8$ and $x_1 = .7$

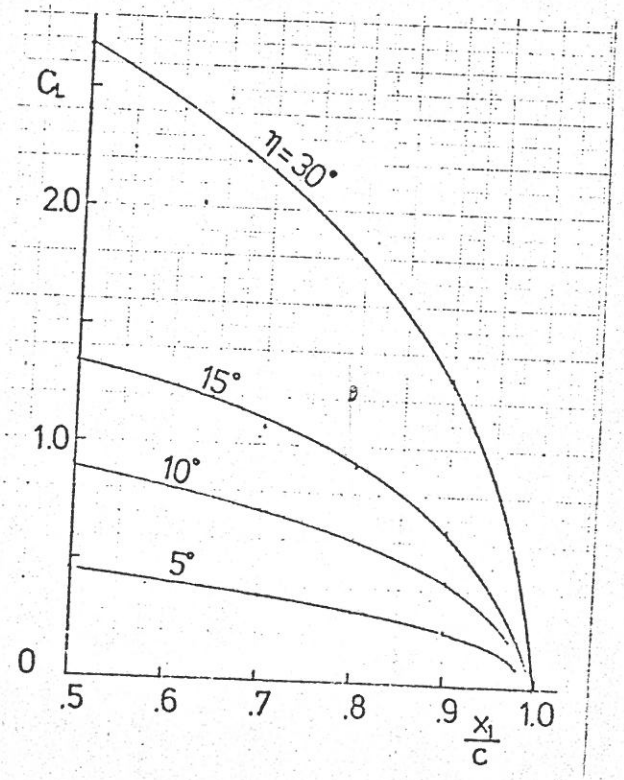

Fig.31 Lift coefficients for $\alpha = \varepsilon$ as function of hinge position x_1 and flap angle

e) Compressibility and shockless flow s auch 6.33

Increasing the freestream velocity to higher subsonic values changes the pressure distribution by a similarity factor. As long as the local Mach number on the surface of the airfoil stays well below 1.0 the Prandtl-Glauert rule says that the compressible Δp and c_p distribution results from the incompressible one by multiplying the latter with $\beta = \frac{1}{\sqrt{1-M_\infty^2}}$ correspondingly the c_L- and c_m-values, but also the pressure gradients go up. For potential flow, however, the drag remains zero and for a real flow practically constant.

To transform the incompressible velocity into a compressible one, there exist several sophistical formula, for instance: the NLR (17) formula

$$V = \left[1 + \beta \frac{(V_i \varkappa - 1)}{B}\right] \frac{1}{\sqrt{1 + \left(\frac{y'}{B}\right)^2}}$$

V_i = incompressible velocity

$B = \sqrt{1 - M_\infty^2 (1 - M_\infty c_{p_i})}$

$y' = \frac{dy}{dx}$

$\varkappa = \sqrt{1 + y'^2}$

When the local Machnumber exceeds the value 1.0 in front of the airfoil crest the flow and drag does not change much. If however the local supersonic field spreads out beyond the crest, the drag will usually sharply increase and the associated Machnumber is called drag divergence Machnumber.

The typical development of the pressure distribution is given in Fig.32. The lower pressures behind the crest constitute a pressure drag. The steep pressure increase at the end of the supersonic field is called shock and resembles to some extent the same phenomena in a one-dimensional flow in a streamtube or Laval-throat. The two-dimensional flow is however basically different and offers the possibility of a smooth return from super- to subsonic flow. The physical interpretation is as follows:

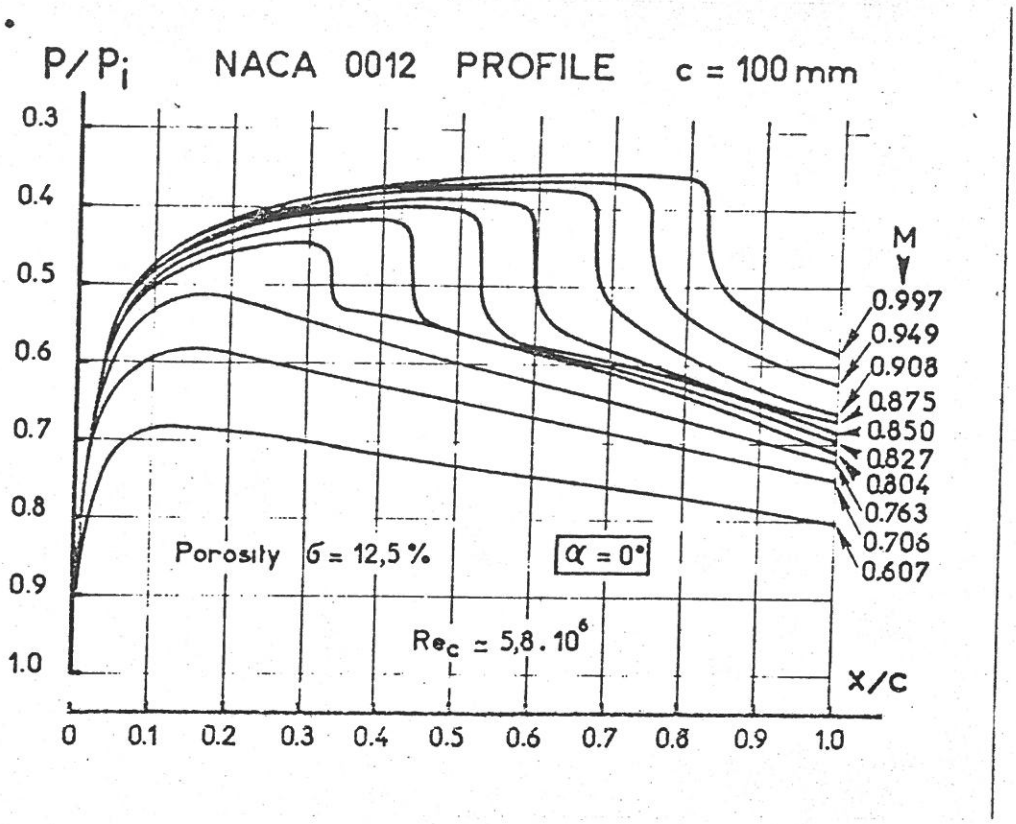

Fig.32 Pressur distributions on the NACA 0012 airfoil at increasing Machnumbers

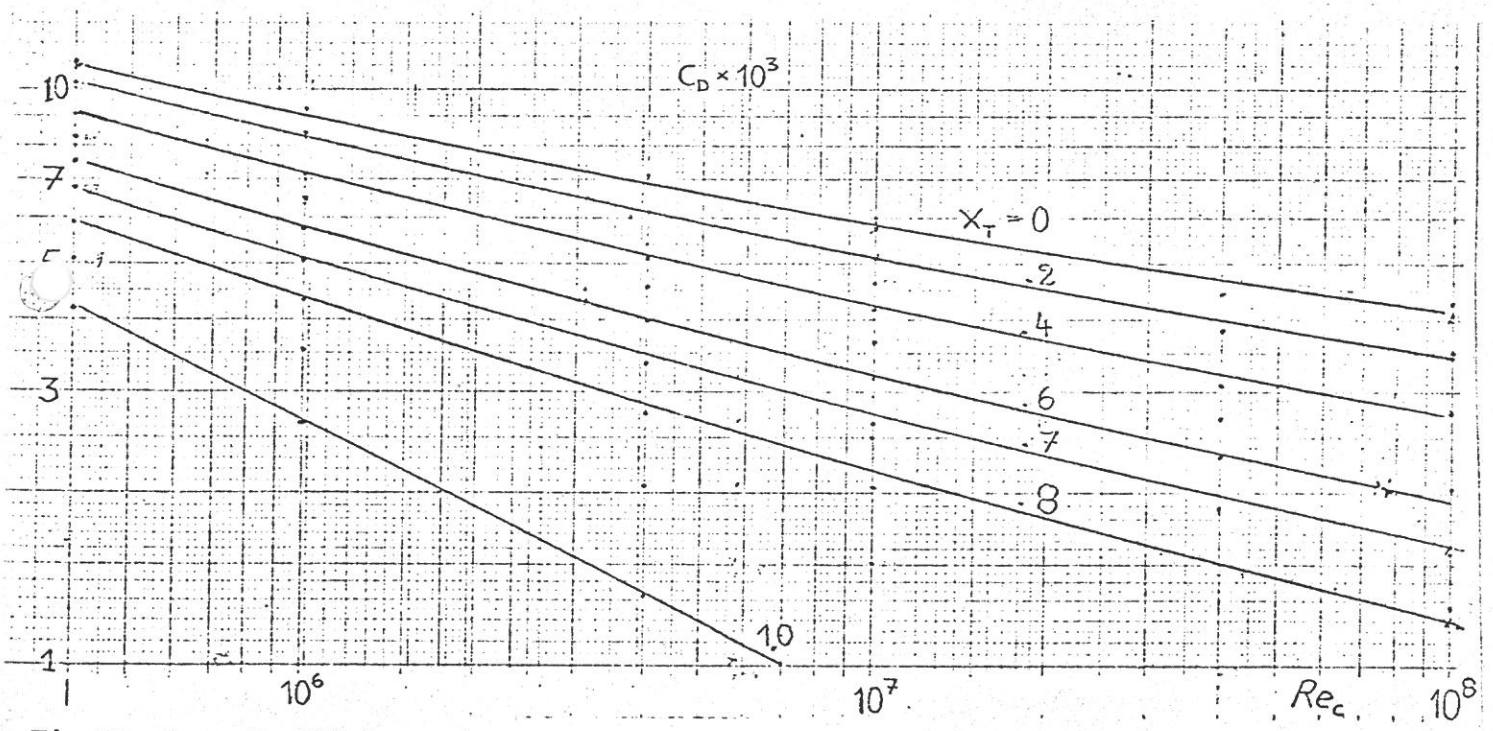

Fig.33 Drag doefficient of flat plate for a different transition position x_T and Reynoldsnumber

On the convex surface near the airfoil the flow may reach the sonic point. Now the curved surface requires an outgoing fan of expansion waves, which at the sonic boundary of the supersonic field are reflected as compression waves. The combined effect of both wave groups turns the flow and has to be compatibel with the surface contour. When the whole system of outgoing and incoming waves is evenly distributed the supersonic flow can be retarded in a continuous fashion and return to subsonic flow without a discontinuity in the pressure distribution or the entropy constant. The pressure distribution then has the same form as for subsonic flow and the pressure drag remains zero.

The possibility of shockless flow was first empirically observed and understood in the sixties by Pearcy (13) and around 1967 Nieuweland (14) showed theoretically the existence of shockless flow for the quasi-elliptical airfoils. With shockless flow the velocities on the surface of airfoils can be higher without a drag penalty.

That means that symmetrical airfoils may be thicker for the same Machnumber or for the same thickness the Machnumber may be higher. For lifting airfoils it means more lift for the same Machnumber or the same lift for a higher Machnumber.

There exists an upper boundary for the maximum local Machnumber inside the supersonic field with $M_L \approx 1.4 \div 1.5$. This fact can be interpreted by considering perturbation waves travelling upstream with sonic speed. Since the flow speed near the airfoil surface and downstream the supersonic field is higher than farther away the waves will turn and entering the supersonic field there is a chance that the flow velocity perpendicular to the wave front is not as large as the speed of sound. Now a sequence of perturbation waves is not stopped at the rear boundary of the supersonic field and does therefore not gather into one single steep perturbation, the shock.

The promising features of shockless or supercritical flow has led in the past decade to a whole spectrum of computational methods for the investigation and the design of such airfoils which cannot be dealed within the framework of this compilation.

III. Examples of airfoils

a) Symmetrical airfoils

The drag of symmetrical airfoils can be calculated by the well-known formula of Pretsch or Squire-Young, see (3) :

$$c_D = 4\left(\frac{\vartheta}{c}\right)_\infty \approx 4\left[\frac{\vartheta}{c}\left(\frac{u}{u_\infty}\right)^{3.5}\right]_{T.E.} \qquad (44)$$

The momentum thickness and the "dumping" velocity at the trailing edge determine the drag. Fig.33 gives the drag values of a flat plate and shows the large influence of the Reynoldsnumber and the transition point on the drag.

It should be noted that the "dumping" velocity u_{TE} has not the strong influence as it seems in Equ.44: a small increase in u_{TE} by Δu reduces the pressure gradient and hence the thickness of the turbulent boundary layer by $\left(\frac{\Delta u}{u_1}\right)^3$, see Equ.(13). In the following it will be assumed that the airfoil surface is perfectly smooth.

1) Reynoldsnumber $4 \cdot 10^6$

We may start with some of the wellknown NACA airfoils, smooth surfaces and a Reynoldsnumber of $4 \cdot 10^6$.

The velocity distribution is given in Fig.20.

The experimental drag values for free and enforced transition are listed in Table III.

Table III

airfoil	$c_D \cdot 10^3$ trans. free	equivalent flat plate x_T	$\frac{c_D}{2c_{Ft}}$	$c_D \cdot 10^3$ fully turbulent	$\frac{c_D}{2c_{Ft}}$
NACA 63-015	5.4	.35	.77	9.6	1.37
64-015	5.1	.41	.728	9.7	1.38
65-015	4.9	.47	.678	9.85	1.40
66-015	4.3	.52	.614	10.0	1.42

The drag of the partly laminar airfoils compared to the completely turbulent flat plate ($c_D = 7 \cdot 10^{-3} = 2 c_{F_t}$) is only 60-80%, and the fully turbulent airfoil has 40% more drag than the turbulent flat plate.

At first I would like to discuss the influence of some modifications on the drag of these NACA airfoils for a fixed position of the maximum velocity and consider three flow features: the laminar flow, the transition region and the turbulent boundary layer.

The favorable pressure gradient up to the velocity maximum certifies at $Re_c = 4 \cdot 10^6$ laminar flow, in fact at this chord Reynolds-number even a constant velocity may produce a transition as far back as 60% of the chord. For the 63-airfoil there is a rounded range between the favorable and the adverse pressure gradient. Any laminar separation bubble in this region will have an extremely small wedge angle and does not disturb in the initial values of the turbulent boundary layer. In contrast, the 66-airfoil exhibits a much stronger deceleration and the laminar separation bubble here will certainly be a bad feature. The velocity distribution in the following turbulent part is practically linear.

Obviously there exist two possibilities to improve the drag.

1a) a better control of the transition with a region which destabilizes the boundary layer without separation. Assuming a stable boundary layer up to the maximum velocity, we need a $\Delta Re_\vartheta \approx 400$ or $\frac{\Delta Re_\vartheta}{\sqrt{Re_c}} \approx .2$ behind this point. According to to Fig.6 this means nearly 30% of the chord.
Sometimes it is not useful to go to the extreme and a shorter instability range may be helpful, since any following separation bubble will be drastically reduced due to the amplified perturbations in front of the separation.

1b) The second possibility aims to a better control of the turbulent boundary layer. Fig.34 gives an example of this idea: for the same transition point at $x_1 = .5$ and $Re_c = 10^7$ the drag of the modified airfoil is some 13% smaller than the drag of the NACA counterpart. The large difference in the boundary layer thickness at the trailing edge is partly canceled by the higher trailing edge velocity of the modified airfoil.

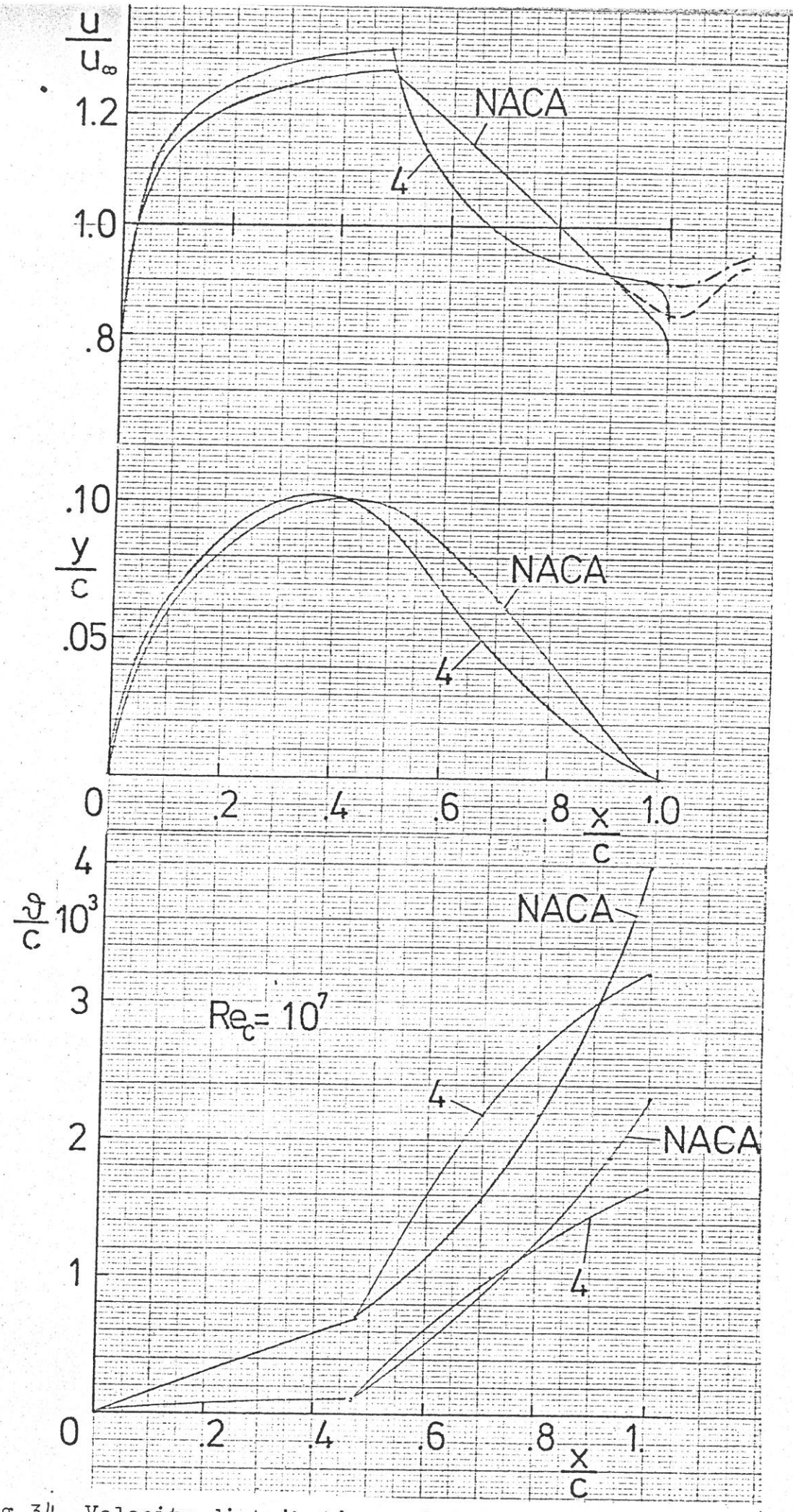

Fig.34 Velocity distribution, airfoil shape for two 20 % airfoils. The boundary layer is calculated for $Re_c = 10^7$ and two transition positions.

In both cases the effect of the displacement thickness on the velocity distribution has been included.

2) Reynoldsnumber $40 \cdot 10^6$

Now we may change the Reynoldsnumber to $40 \cdot 10^6$.

If we approximate the velocity distribution in the forward part by $U \sim x^m$ with $m = +.05$ we have $re_{\vartheta_{crit}} \approx 600$ which will be reached at 5% of the chord. In reality the acceleration is usually higher, and the instability point further aft, compare Fig.4. In order to certify a transition in the 30 to 40% chord position it is necessary to strengthen the favorable pressure gradient. With $m = +.1$ the critical chord position is nearly 8% and with a $\Delta re_\vartheta \approx 1500$ the transition can go to the desired position. Now we do not need any destabilizing link and can immediately start with a concave distribution for the turbulent boundary layer.

3) Reynoldsnumber $0.4 \cdot 10^6$

$\frac{\Delta R_{\delta_2}}{\sqrt{Re_c}} = 0.237$

For the low Reynoldsnumber the velocity distributions of Fig.20 are no longer adequate. Experimental results show that now the velocity distribution of the NACA 0012 type is one of the best. The reason is quite obvious: after Granville we need at least a $\Delta re_\vartheta \approx 400$ and $\frac{\Delta re_\vartheta}{\sqrt{Re_c}} \approx .6$ and Fig.6 tells us that nearly the whole chord length is necessary for the instability range. Practically it is hard to provoke transition without separation.

The drag of the 0012 at this Reynoldsnumber is $6.8 \cdot 10^{-3}$ or 62% of the turbulent flat plate. To produce this drag on a flat plate the transition has to be at 70% chord. On the 0012 the laminar separation point is also near 70%.

Can we conceive a variation of the velocity distribution which may reduce the drag a little more? Fig.35 gives an alternative, which avoids separation and transition up to 80% of the chord.

b) Low drag bucket

For Reynoldsnumbers between $1 \div 10 \cdot 10^6$ airfoils as in Fig.20 develop a typical low drag range with a considerable drag increase at the edges. This is a consequence of the angle of incidence which changes the velocity distribution similar to Fig.23 by an additional gradient. This has the effect that on one side the stability is enhanced more than necessary and reduced on the other side.

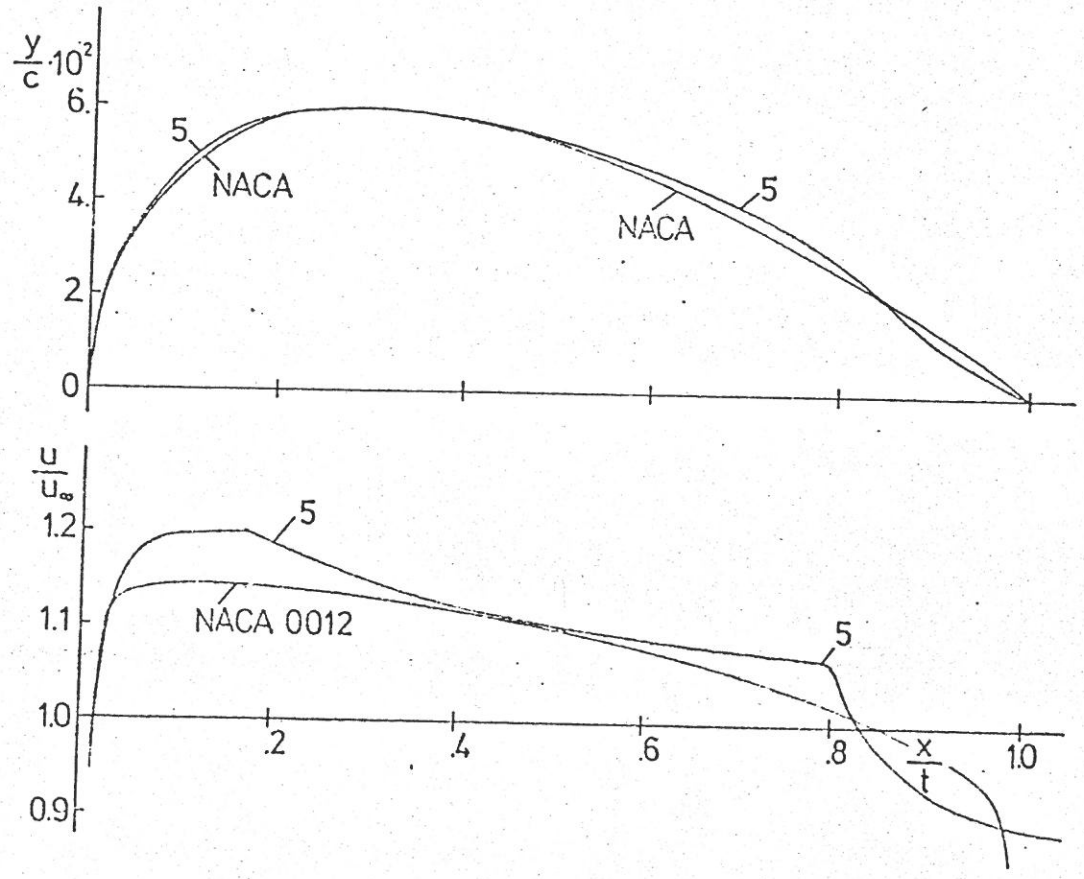

Fig.35 Velocity distribution and airfoil shape of the NACA 0012 and a modification for $Re_c < 10^6$

At a certain α and c_L the transition jumps forward on one side and creeps back very little on the other side. The drag then increases also sharply.

The width of the low drag bucket depends obviously on the size of the basic pressure gradient in the front part of the airfoil. A large gradient can stand higher Δx before the boundary layer stability is lost. Therefore in Fig.20 the 63-airfoil must have wider low drag buckets than the 66-airfoil at the same thickness. This is a statement which is valid for all types of "laminar" airfoils.

We may change the type of airfoil as in Fig.20 and fix the Reynoldsnumber and thickness or we fix the airfoil type and Reynoldsnumber and change only the thickness or we have only one airfoil and change the Reynoldsnmuber. Fig.36 gives an evaluation of some symmetrical NACA 6 series at $Re_c = 6 \cdot 10^6$.

How are the low drag airfoils designed?

For the front part of the airfoil it is reasonable to search for a velocity distribution ~~which~~ ose gradient does not change sign up to a certain angle of incidence and chordwise position, where the instability range or pressure increase begins. With other words, there should be a constant velocity at a certain incidence and below this the velocity should monotoneously increase. It is not difficult to write a computer program which investigates the velocities at different angles of incidence, and to correct the input velocity to get a fast converging solution for such distributions.

Outside the low drag bucket the drag increases steadily with higher angles of incidence. The steepness of the drag increase depends heavily on the Reynoldsnumber and thickness.

For a Reynoldsnumber below 10^6 the optimum velocity distribution has to be more of the 0012 type. Now with angle of incidence the transition moves on side forward and by nearly the same amount backwards. There exists low drag but there is no sharp increase in drag with growing angles of incidence. If we exclude the low drag bucket, the drag due to lift increases with Δc_L^2 as long as the flow is attached. For $Re \approx 10^7$ and $\zeta \approx .12$ the drag is practically doubled at a $\Delta c_L = 1.0$.

c) Airfoils with low drag bucket and small camber

If we apply the NACA a = 1.0 meanline to symmetrical airfoils the pressure gradients are not changed, only the Re-number of the laminar boundary layer is slightly modified. Therefore the transition position as well as the drag will be similar to the symmetrical counterpart and the momentum thickness at the trailing edge is practically the same.

The drag coefficient for this case is

$$c_D = 2\left[\underset{\text{upper side}}{\frac{\vartheta}{c}\left(\frac{u}{u_\infty}\right)^{3.5}_{T.E.}} + \underset{\text{lower side}}{\frac{\vartheta}{c}\left(\frac{u}{u_\infty}\right)^{3.5}_{T.E.}}\right] \qquad (45)$$

With equal ϑ on the lower and upper side at the trailing edge and replacing $(u^{3.5})$ by (u^3) we get

$$c_D \approx 2\frac{\vartheta}{c}_{T.E.}\left[\left(\frac{u}{u_\infty}\right)^3_{up} + \left(\frac{u}{u_\infty}\right)^3_{low}\right] \qquad (46)$$

Now for thin airfoils is

$$\left(\frac{u}{u_\infty}\right)_{up} \approx 1 + \frac{\Delta u}{2}$$

$$\left(\frac{u}{u_\infty}\right)_{low} \approx 1 - \frac{\Delta u}{2}$$

if Δu is the total difference in U between upper and lower side.

If c_{D_o} is the drag coefficient for the symmetrical airfoil the cambered airfoil has

$$c_D \approx c_{D_o}\left[1 + 3\left(\frac{\Delta u}{2}\right)^2\right] \qquad (47)$$

For $c_{L_i} = 1$ and $\frac{\Delta u}{2} = .25$ the value of the parenthesis becomes $1 + .187$. For this highly cambered airfoil the additional drag due to camber is nearly 20%. For a $c_{L_i} = .5$ it becomes only 4%.

Therefore all results of the symmetrical airfoils may be transformed to cambered airfoils with a small drag penalty near the c_{L_i}.

Outside the low drag bucket the drag polar of cambered airfoils is no longer symmetrical. On the upper side the additional drag is more heavily weighted than on the lower side and this difference increases with camber.

d) Symmetrical airfoils with flap

Symmetrical airfoils are mostly used for rudders. As such they usually have a flap. Sometimes the flap is deflected for a large part of the operation time. Then it makes sense to ask for an airfoil which has a favorable pressure distribution for the deflected flap.

In general an ordinary airfoil with a plain flap does not possess this quality. Fig.37 gives a typical example with the NACA 64-012 airfoil. The surface is smooth and $Re_c = 10^6$. On the left hand the drag polar of the airfoil is given with a .25% flap chord and a flap angle $\eta = 15^o$. The Σ form of the drag polar is not a special feature of this particular airfoil, but a rather typical feature.

The drag increase above $C_L = .8$ and below $C_L = 0$ is mainly due to the transition jump to the nose on the "outer" side. Starting at $C_L = .9$ the drag reaches to the minimum when the transition position goes to the hinge line. Then for lower C_L the boundary layer separates laminar forming a bubble on the upper side of the flap.

It is most remarkable that for decreasing α the transition position on the upper side remains practically unchanged, the boundary layer thickness behind the reattachment point however changes in the same way as the drag or the boundary layer close the trailing edge.

To be sure that no appreciable contribution to the drag comes from the lower side, also the transition here was observed. What causes the strong drag variation for lower lift coefficients? There can be only one reason: the changing separation angle in the laminar separation bubble or more precisely: the height of the transition nucleus above the airfoil surface determines the initial thickness of the following turbulent boundary layer.

Why does it change this way?

From Fig.29 and 30 it can be seen that behind the hinge line there exist in potential flow strong velocity gradients, the separation angle of the bubble must be large at $C_L = .8$. For lower C_L the laminar boundary layer becomes more stabilized and the transition goes slightly back causing a strong effect on the turbulent boundary layer. For C_L-values below .5 the transition position is un-

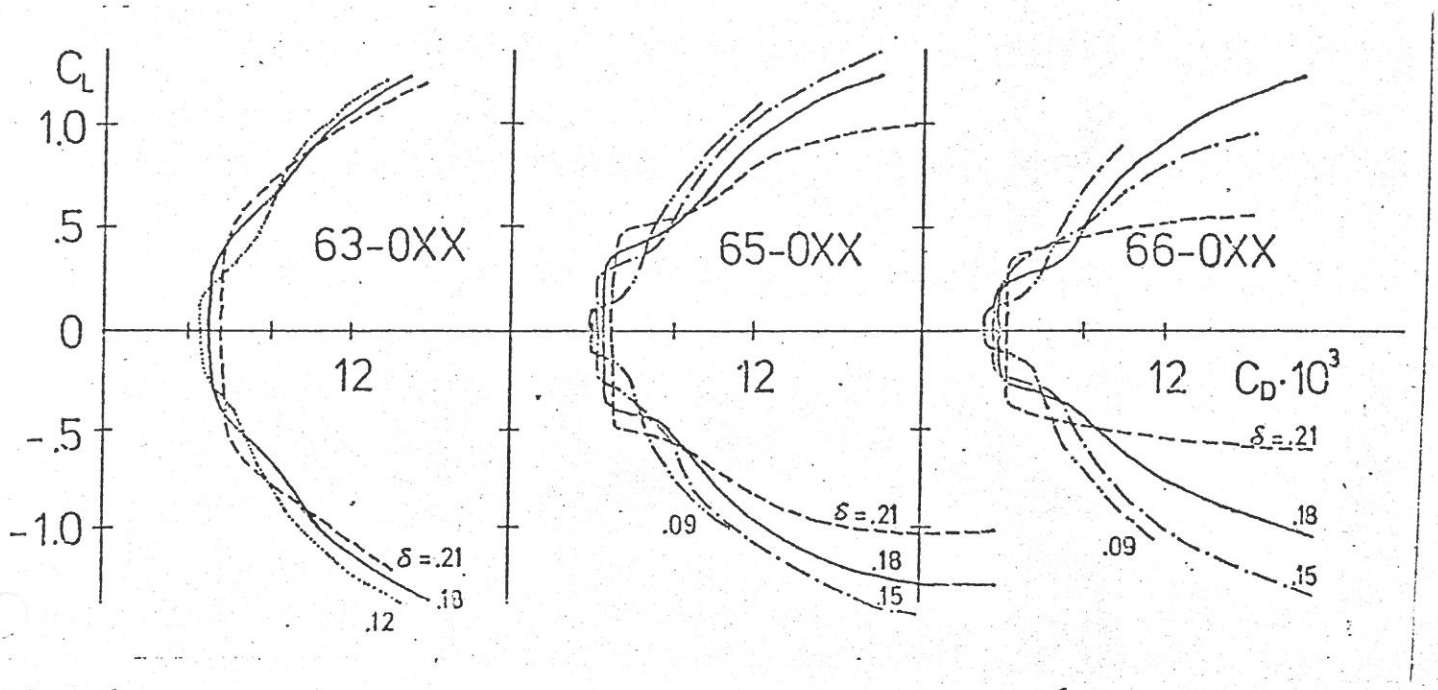

Fig.36 Drag polars of different airfoils at $Re_c = 6 \cdot 10^6$.
Narrow buckets with low drag and wider buckets with higher drags establish an common envelope

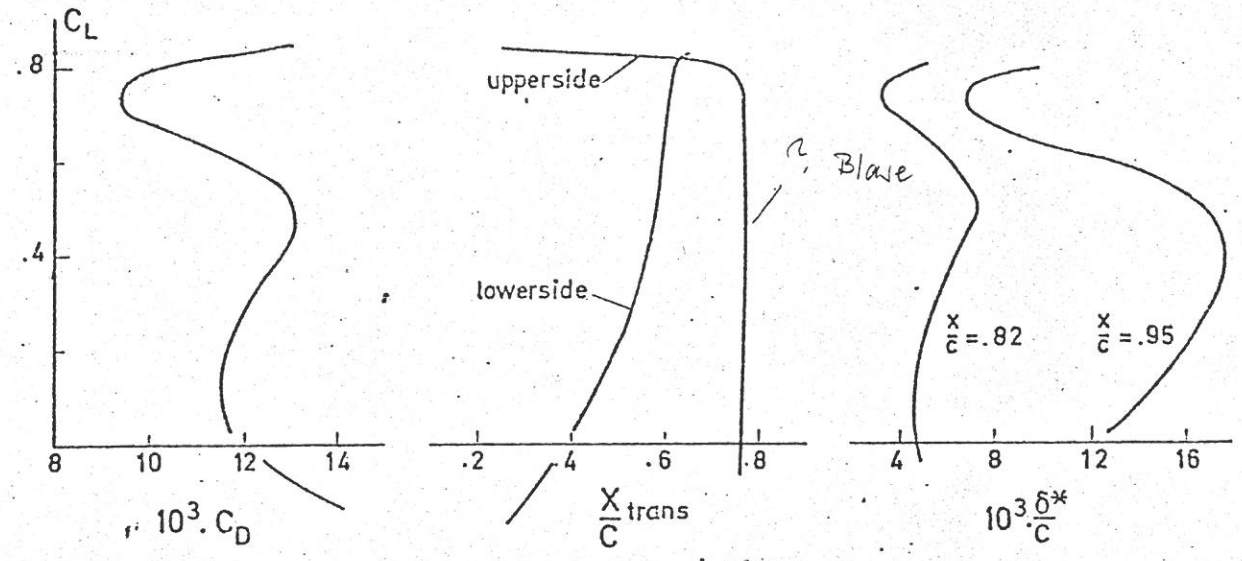

Drag, transition and boundary layer displacement thickness of the NACA 64-012 with 15° flap angle. Re = 1.0 . 10^6.

Fig.37

changed, but the overall pressure gradient behind the hinge is greatly alleviated. Causing a smaller separation angle and better initial conditions for the turbulent boundary layer, the drag becomes again smaller to reach the second minimum before the transition shifts on the lower side.

This situation may be improved (15) if we can control the velocity distribution and hence the transition and the turbulent boundary layer. This can be done in a similar way as designing a "laminar" airfoil. At first a symmetrical airfoil is generated, then the flap is deflected and this cambered version is analysed to check the velocity distribution. This output is corrected with respect to laminar boundary layer stability and transition control. The correction goes to the original input and so on.

Fig.38 gives a result and a comparison with the NACA 64-012. The most striking feature of the airfoil shape is the concave kink at the hingeline, which makes for a smooth "upper" side if the flap is deflected by small angles, say 10-12 degrees. More subtle changes are in the nose region to counteract the velocity peaks associated with the flap deflection.

Fig.39 gives the drag polar of both airfoils and shows that at the same drag the width of the low drag bucket is a little larger for the FX airfoil. Deflecting the flap simply shifts the whole drag polar to positive c_L without any irregularities.

e) Transonic airfoils

s. auch S. 25

Transonic flow will develop when the local Machnumber on the surface exceeds values over one. For freestream Machnumbers above .75 this is already the case if the c_p-value reaches values of $c_p = -.8$. In terms of airfoils this needs only a thickness near $d = .12$ and a small angle of incidence. For a freestream Machnumber of .5 as happens on the retreating blade of a helicopter rotor a $c_p = -2.1$ is necessary, which means an angle of incidence around 10° and c_L around 1.0. Even for a freestream Machnumber of .2 local Machnumbers of one may be reached if on the slat of a multielement high lift configuration the c_p-value goes to $c_p = -16$.

The local supersonic field is usually terminated by a shock, a steep pressure increase, which leads very soon to a drag divergence. The drag is caused by the entropy increase in the shock,

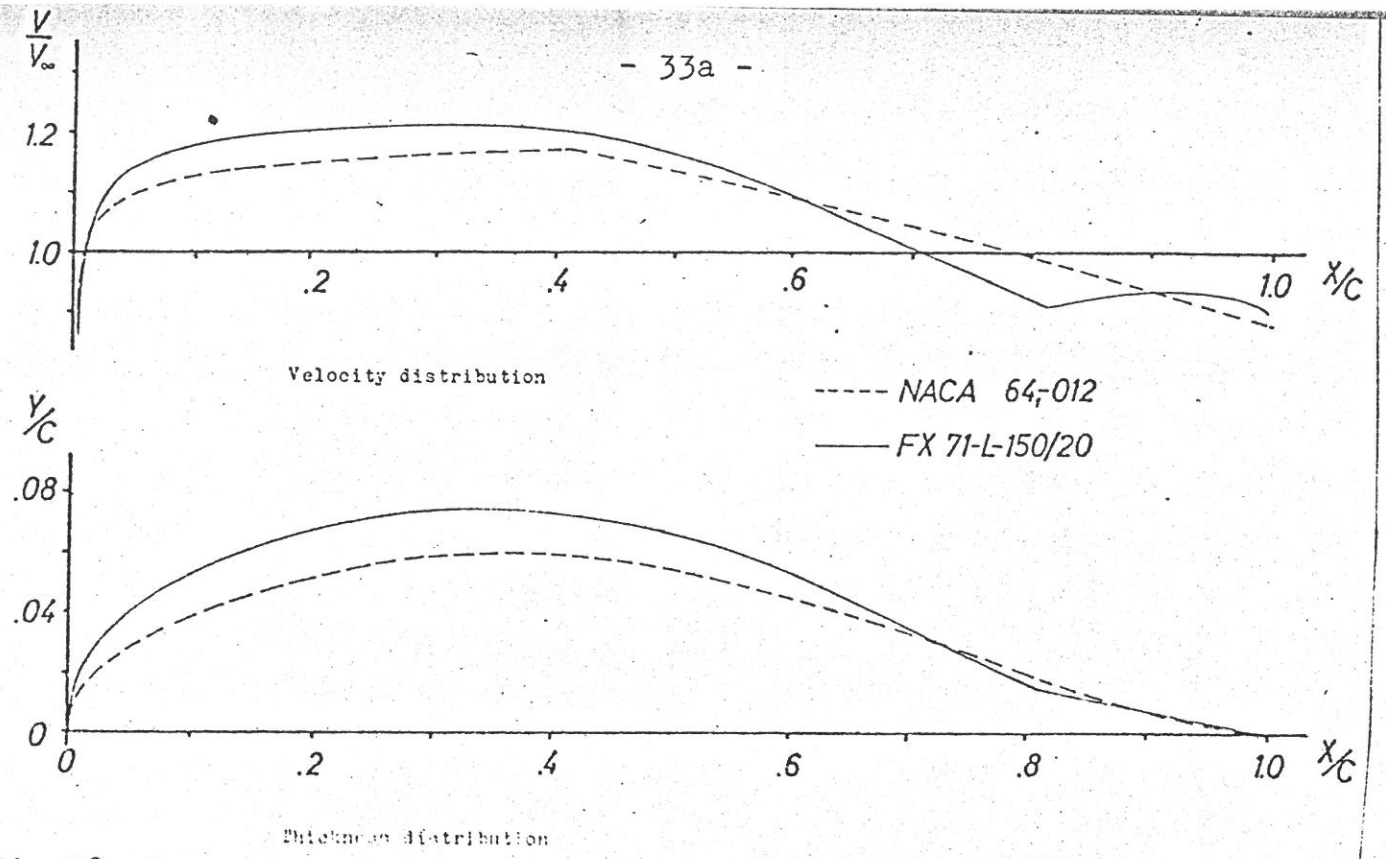

Fig.38 Comparison of shape and velocity distribution of the NACA 64-012 and an FX airfoil optimized for a flap chord of 20 % and η = 10°

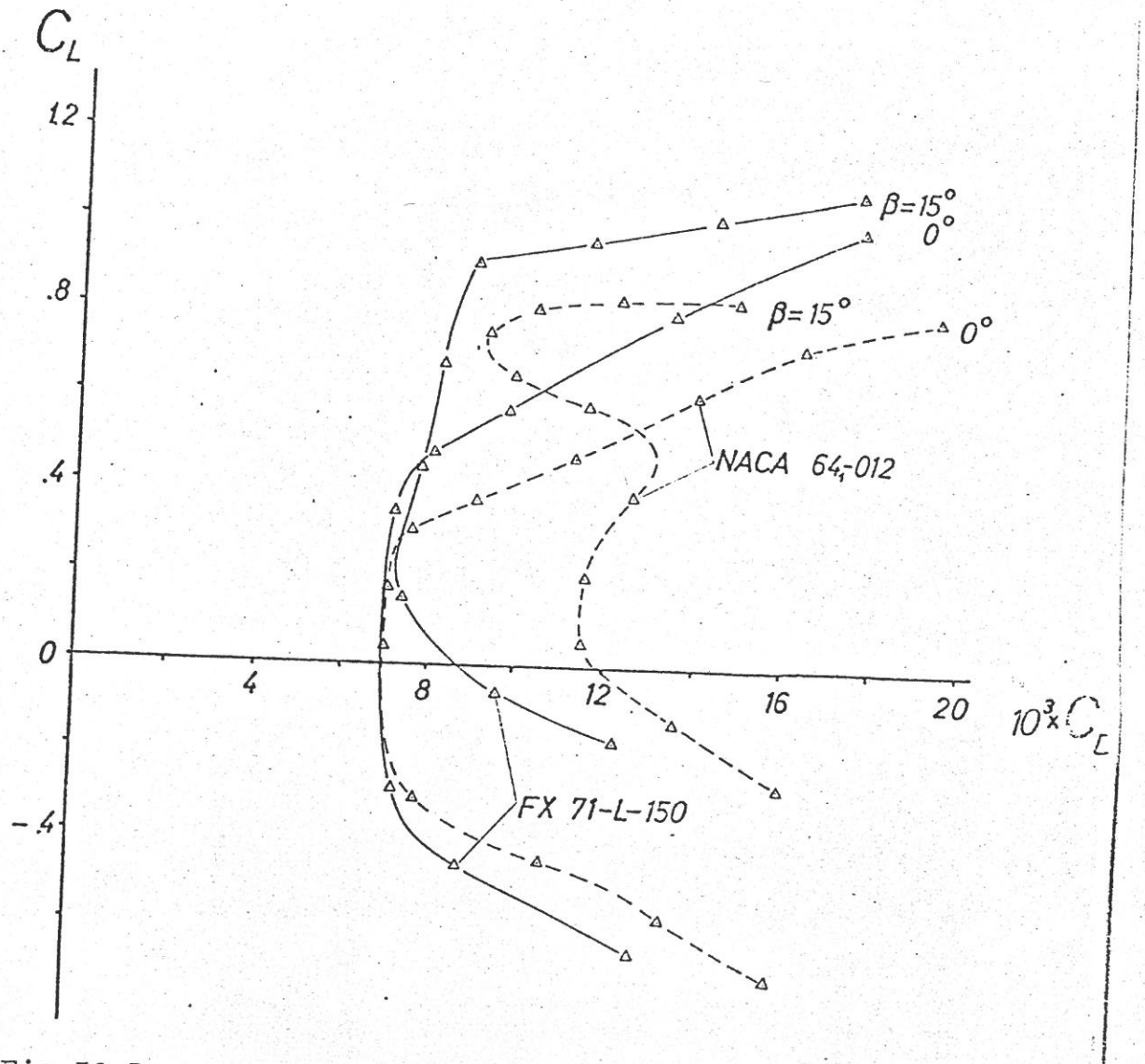

Fig.39 Drag polar of the NACA 64-012 with a 25 % flap and a FX airfoil with a 20 % flap. $Re_c = 10^6$

transferred to the airfoil via the pressure distribution and by the interference with the boundary layer which looses very soon its ability of pressure recovery.

The Machnumber therefore puts a more severe constraint to the airfoil flow than any other parameter.

There are two possibilities to shift the drag divergence Machnumber to slightly higher values, say $\Delta M_{cc} \approx .05$. The first tends to avoid a supersonic field at all by reducing the top velocity on the airfoil upper surface as much as possible: the airfoil thickness is reduced to the structural minimum and the thickness is evenly distributed along the chord to get a roof top type of airfoil. Finally, the lift distribution is shifted to the rear, where the thickness contribution to the supervelocity diminishes (see Fig.25). Since this implies high pitching moments and some trim drag, it is a good example for the willingness to trade anything, if the drag divergence Machnumber could be increased a little.

The second possibility may retain all the advantages of the first type but strives additionally to allow for supersonic fields without shocks at higher freestream Machnumbers. The fact that such flows are possible at all was long doubted until a decade ago Nieuveland (14) gave an exact solution for such shockless flows. Certainly there were many experimental observations before, especially in England by Pearcy (13), which evidenced the same fact to a more or lesser degree.

Shockless flow is basically a potential flow quality which physically can be understood as a well structured local supersonic field: At the forward sonic point of the supersonic field on the convex airfoil surface expansion waves go out and are reflected at the sonic line above the airfoil as compression waves. Both waves groups turn the flow direction along the curved surface and there is no reason why the compression waves should not be able to cancel the total expansion completely. The pressure distribution then looks as a subcritical distribution and in potential flow there is no drag. Obviously, such a flow field is a special solution of the underlaying potential equations, holding only for a certain combination of airfoil form, angle of incidence and freestream Machnumber. For off-design conditions the internal

structure of the supersonic field will not suddenly break down, however the pressure recovery will be less perfect and shocks of increasing strength will appear. The interaction between potential flow and boundary layer is sometimes much stronger due to the delicate nature of the flow behaviour near $M_\infty \approx 1$.

With respect to boundary control, to strive for a shockless flow is in general the best one can do.

However, not every shockless airfoil is also a good airfoil, because any "good" airfoil has to have some "forgiving" qualities outside the design condition. This means that the airfoil should have some margins before the interference between the shock and the boundary due to higher freestream Machnumber or higher lift establishes the inacceptable buffeting limit.

Fig.40 shows the typical changes in the pressure distribution due to off-design conditions. From the infinite number of solutions it seems that the so-called "peaky" airfoil, where the supersonic field is mostly in front of the airfoil crest is less sensitive to off-design conditions than others. Fig.41 illustrates the idea "peaky" which means a concave distribution between $c_{p\,min}$ and the crest.

To calculate shockless airfoils there exist today many methods, which are powerful, mostly reliable, but also expensive. For design purposes, especially when the design procedure is complicated by conflicting requirements, as for instance with the helicopter airfoil, it is sometimes useful to have available as a first approximation a simple analysis, which was proposed by Pearcy (16).

Given an incompressible velocity distribution and the slope $\frac{dy}{dx} = \phi$ of the airfoil surface, this distribution can be transformed by several formulas into a compressible one. The NLR formula (17) may be applied even for weak supersonic speeds. If this is true, we understand the supersonic field as caused by the total effect of the expansion waves e(x)

$$E = \sum_{x_{sonic}}^{x} e(x)$$

and the compression waves c(x), yielding

$$C = \sum_{x_{sonic}}^{x} c(x)$$

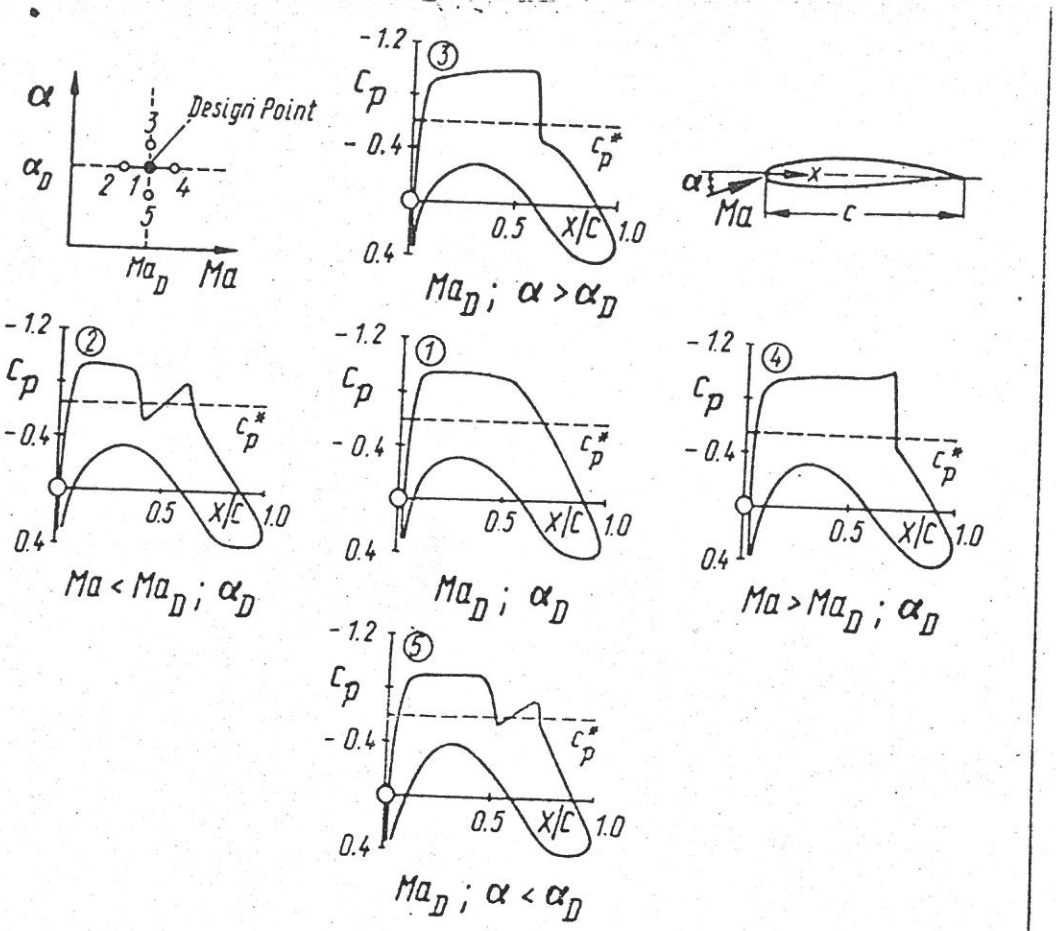

Fig.40 Typical changes of the design pressur distribution due to $\pm \Delta\alpha$ or $\pm \Delta M_\infty$

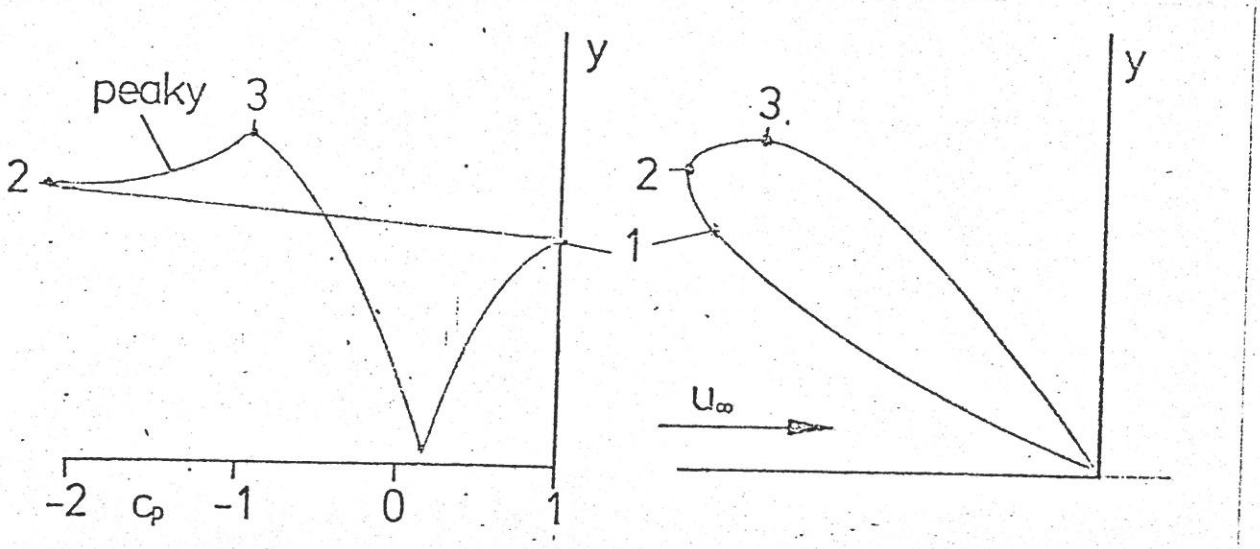

Fig.41

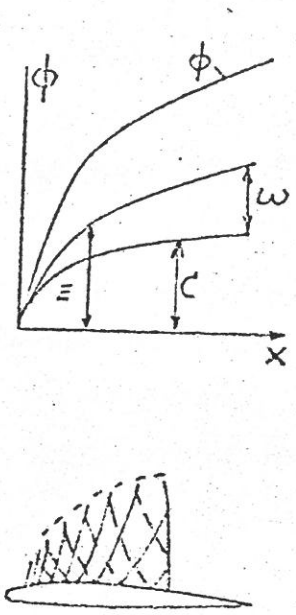

Fig.42

which together determine the flow direction ϕ at the surface, see Fig.42.

The difference between E and C constitutes the effective Prandtl-Meyer angle ω which causes the supersonic velocity. For a shockless flow it is necessary, see Fig. 43, that ω diminishes smoothly to zero near the crest. This condition is here always satisfied and alone not sufficient. As has been pointed out earlier the velocity inside the supersonic field has to stay below a maximum local Machnumber, say 1.4 - 1.5, or the ω-values should not exceed 12 degrees. Another additional condition is to avoid that the reflected compression waves coalesces inside the supersonic field, which may happen when the expansion curve E(x) doesn't have a monotoneous increasing distribution.

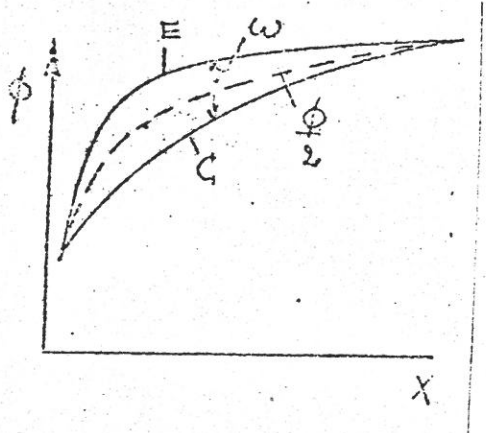

Fig.43

The internal structure of the supersonic field is the result of the airfoil shape and the velocity distribution. There remains the question how to correct the airfoil in order to go from Fig.42 to Fig.43. It seems that the velocity corrections play the most important part and the associated changes of the airfoil shape do not disturb the fast converging iteration.

Airfoils for the helicopter rotor put a special problem of transonic flow, which is different from the single purpose design of a fixed wing aircraft. The most critical conditions emerge from the high speeds on the advancing side and from the high angle of incidence on the retreating side of the rotor and additionally by the general requirement of a rigid airfoil with zero pitching moment.

Fig.44

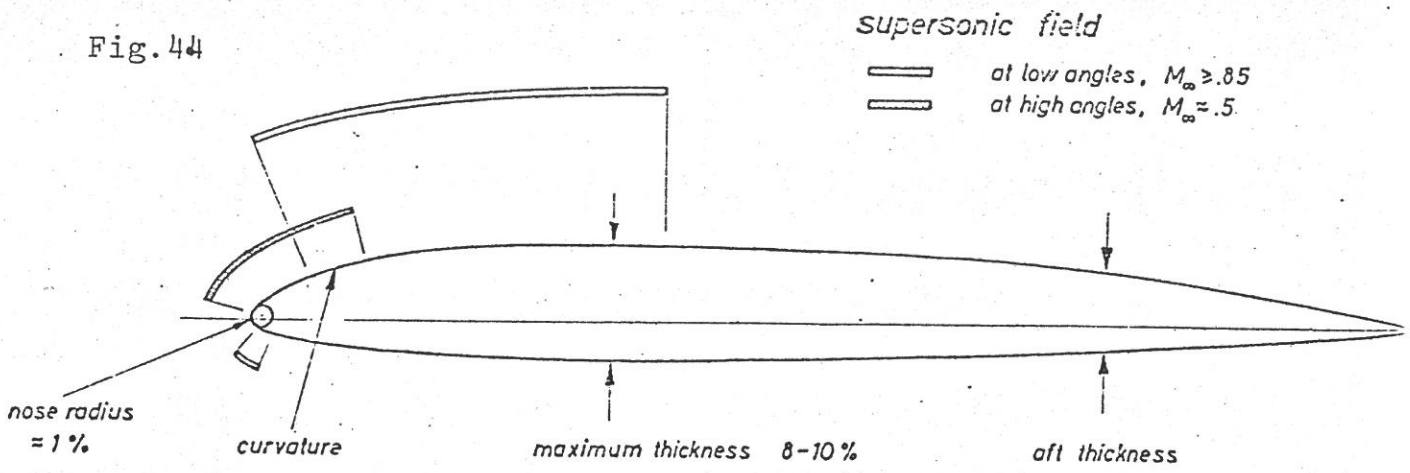

Fig.44 shows the typical form of a rotor airfoil and the most critical regions. For the high speed case these are on the upper side and on the lower side very close the nose. For high angles of incidence the upper nose region is critical.

In the following the results of the simple analysis, which was originally used for the selection process, are compared with later results of the Garabedian-Korn methods. For the high speed case Fig.45 and 46 compare for the same airfoil the results of the mentioned simple analysis and the pressure distribution due to the Garabedian-Korn method. Fig.45 shows that the upper side of this airfoil is not well suited for Machnumbers above .75 and angles of incidence higher than -1.41 degrees. The Garabedian method in Fig.46 indicates for α = -1.9 degrees and M_∞ = .79 the first appearance of shocks on the upper and lower side and a wave drag of $6 \cdot 10^{-3}$.

In Fig.47 and 48 the same airfoil is compared at high angles of incidence and M_∞ = .5. Again the simple analysis indicates that at this Machnumber an angle of attack α = 9.8 degrees is somewhat above the allowed $\omega \approx 12^\circ$ and Fig.48 confirms this expectation. Therefore the simple analysis of Pearcy is an appropriate method and convenient for a first selection step.

f) Fully turbulent airfoils

The minimum drag of fully turbulent airfoils can most conveniently be described by

$$c_D = 2 c_{F_t} \left[1 + 2{,}5\, \delta + 60\, \delta^4 \right] \qquad (48)$$

Here c_{F_t} means the surface friction coefficient of the turbulent

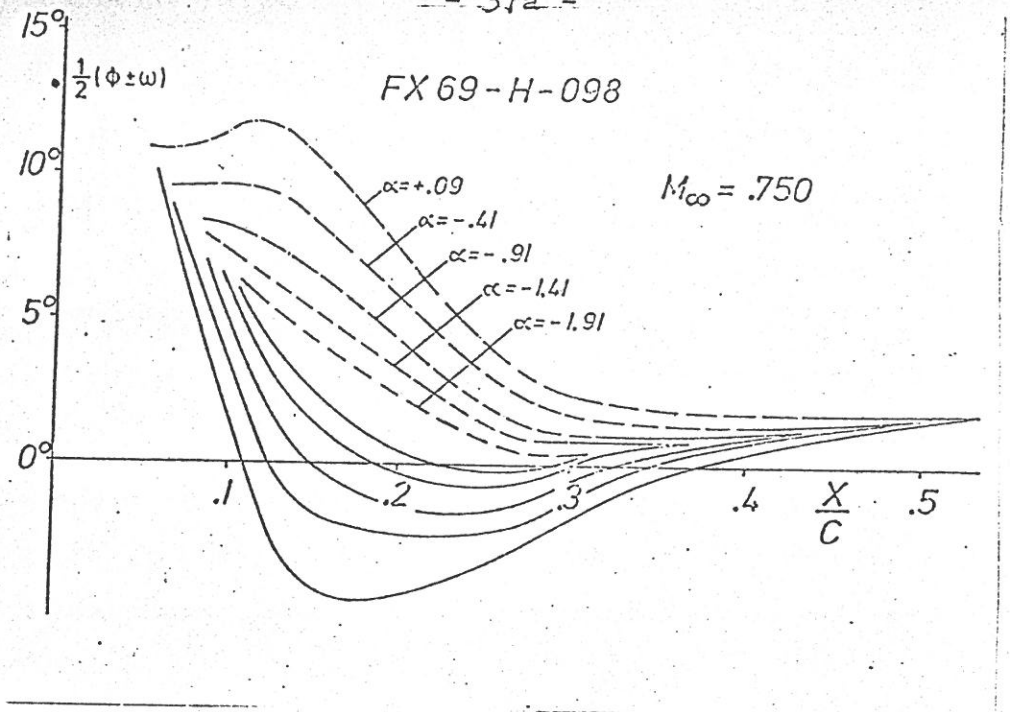

Fig.45 Expansion and compression (dotted lines) distribution along the upper surface of the FX 69-H-098 airfoil. Small α ; M_∞ = .75

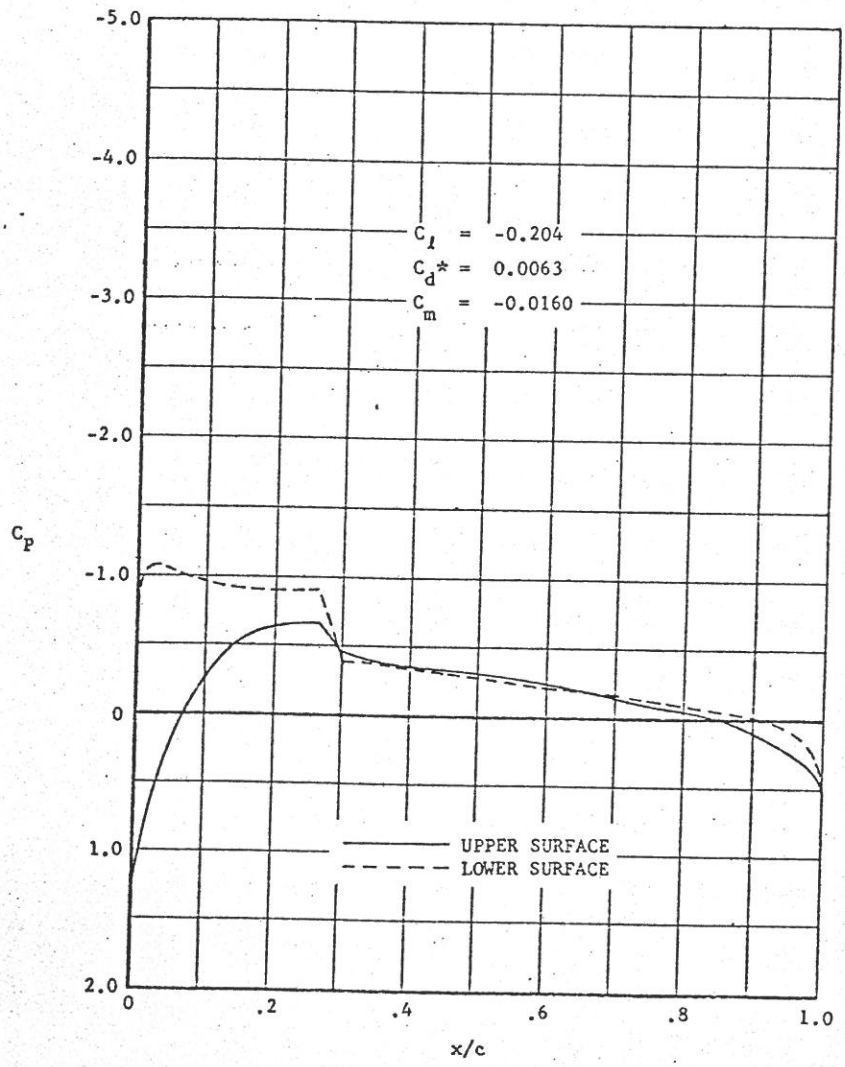

Fig.46 Potential pressure distribuion due to the Garabedian-Korn method for the FX 69-H-098. $\alpha = -1.9^\circ$, $M_\infty = .79$

flat plate and δ the airfoil thickness. Now the airfoil shape or velocity distribution looses its significance on the drag. Only the thickness δ and certainly the roughness of the surface are of importance.

Fig.49 shows the velocity distribution and the shape of three different airfoils with δ = .15. The drag calculated for a transition of $\frac{x_T}{c}$ = .05 at $Re_c = 10^7$ including the wake effect is for all three airfoils practically the same, see Table IV. It seems that for fully turbulent flow a position of the maximum thickness near the 40% chord point has a small advantage.

Table IV

Airfoil	$C_D \cdot 10^3$	$C_D/2C_{Ft}$	δ
1	8.36	1.417	.15
2	8.42	1.420	.15
3	8.58	1.450	.15
4	9.32	1.58	.2
NACA	9.52	1.613	.2
2 C_{Ft}	5.9	1.0	0.

The lift dependent drag is more or less quadratic with ΔC_L. As long as the Machnumber or the cavitation limit are not restrictive, the intensitivity of the drag may be used to produce other features which favour the high lift or the stall behaviour.

Fig.50 gives an example: for an VTOL airplane the discharge of the jet engine should be widely deflected by a cascade with a large space/chord ratio. Since a flapped airfoil was acceptable an airfoil of the form shown in the insert of Fig.50 was chosen. The "Cocacola" bottle form favours the flow for the deflected flap and does not change the drag at small flap angles because the turbulent boundary layer is not sensitive to such irregularities, as seen in Fig.50. The drag of the bottle airfoil was $1.25 \cdot 10^{-2}$ and for the other airfoil $1,3 \cdot 10^{-2}$ at $Re_c = 10^6$.

The wings of modern transport airplanes are practically fully turbulent. Mostly due to slat at the nose. The Machnumber is the predominant selection factor, which leads to thin airfoils between 9-12% thickness. These in turn are not able to make full use of the powerful high lift devices at the trailing edge without the help of the slat at the nose.

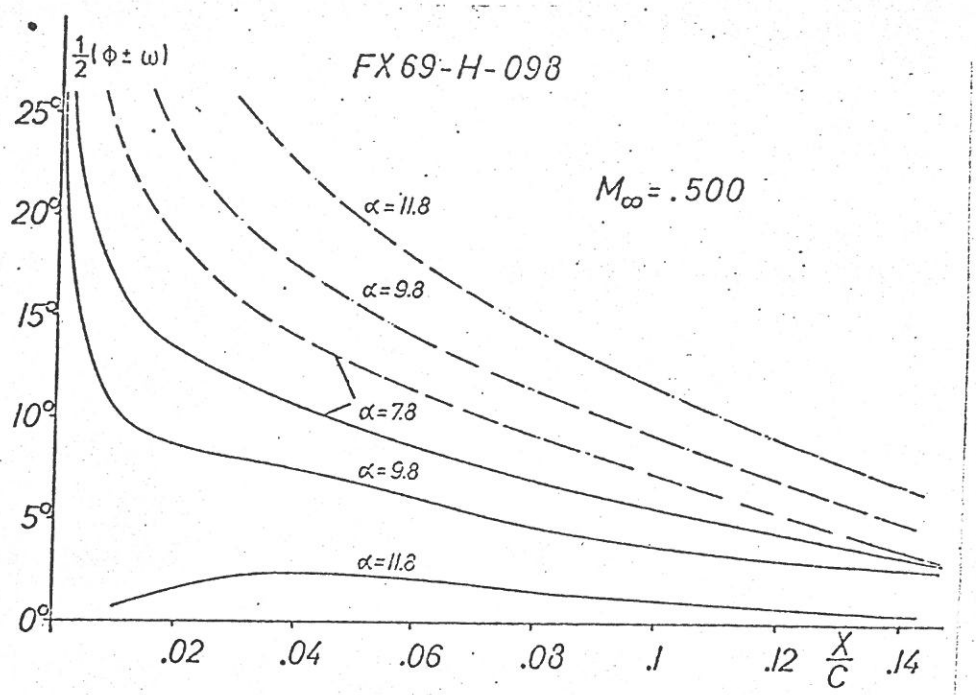

Fig. 47 Expansion and compression (dotted lines) distribution along the upper surface of the FX 69-H-098 airfoil at $M_\infty = .5$ and high angles of attack.

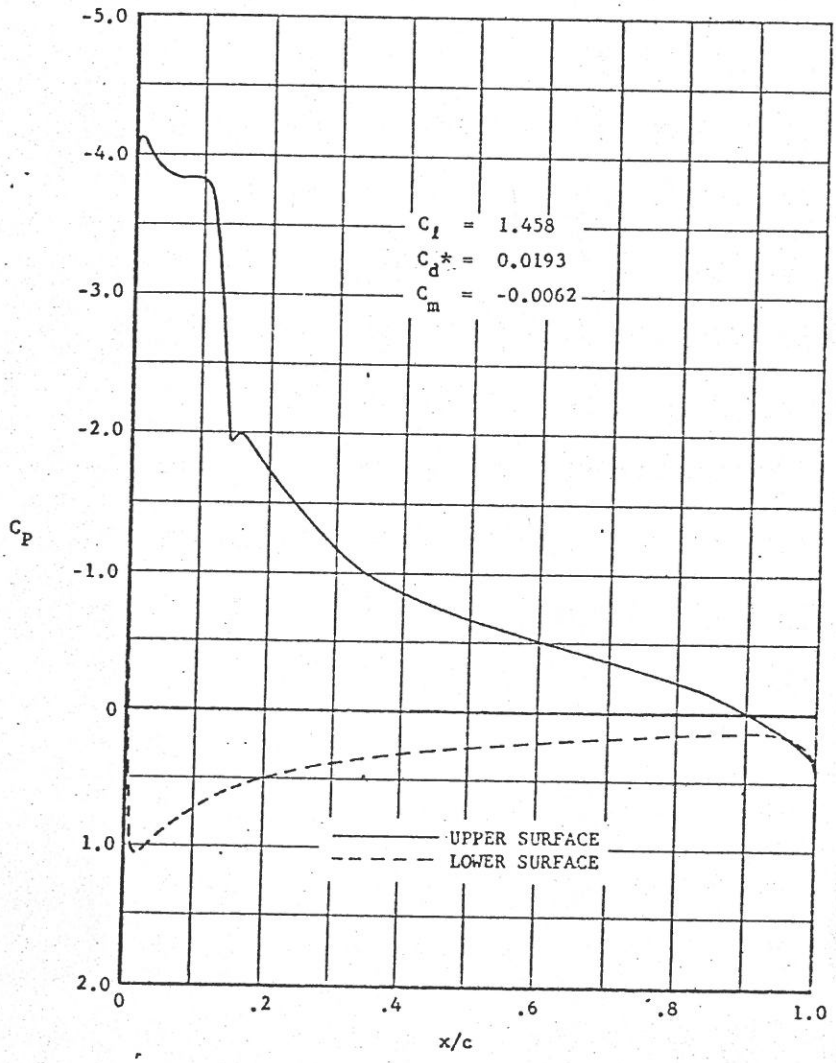

Fig. 48 Potential pressure distribution due to the Garabedian-Korn method for the FX-H-098. $M_\infty = .5$, $\alpha = 9.08$

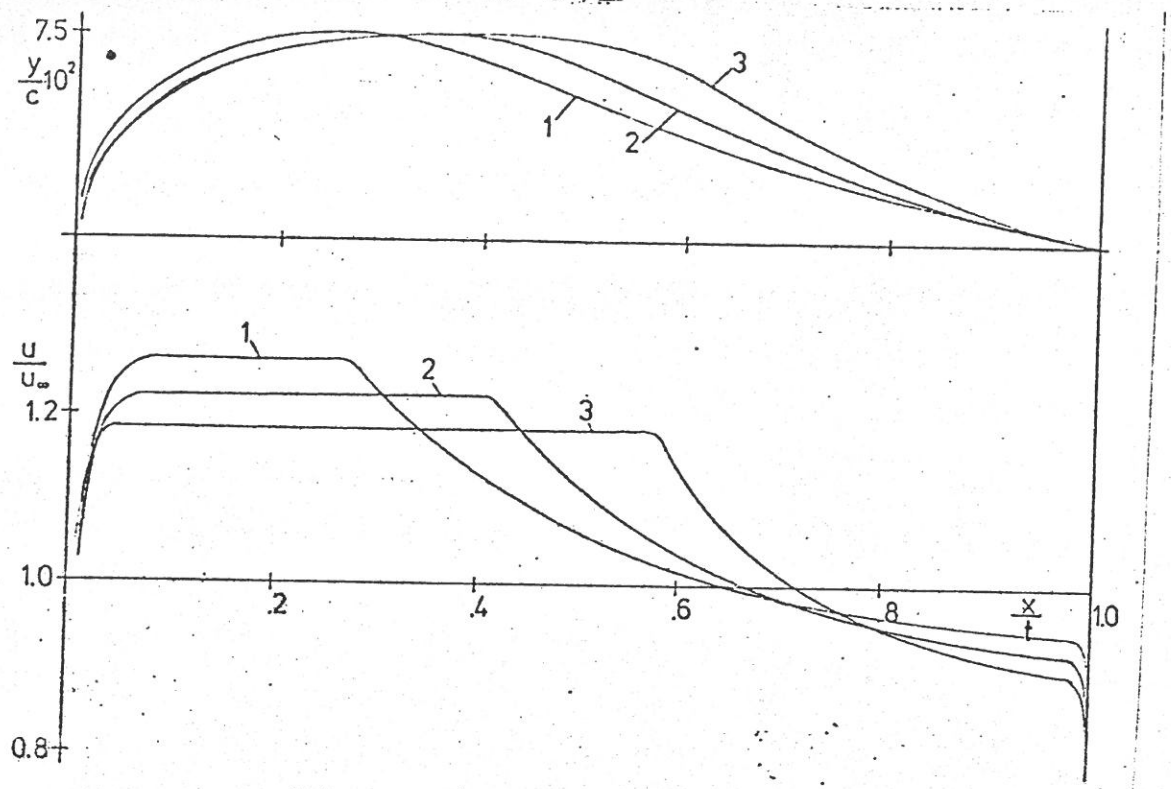

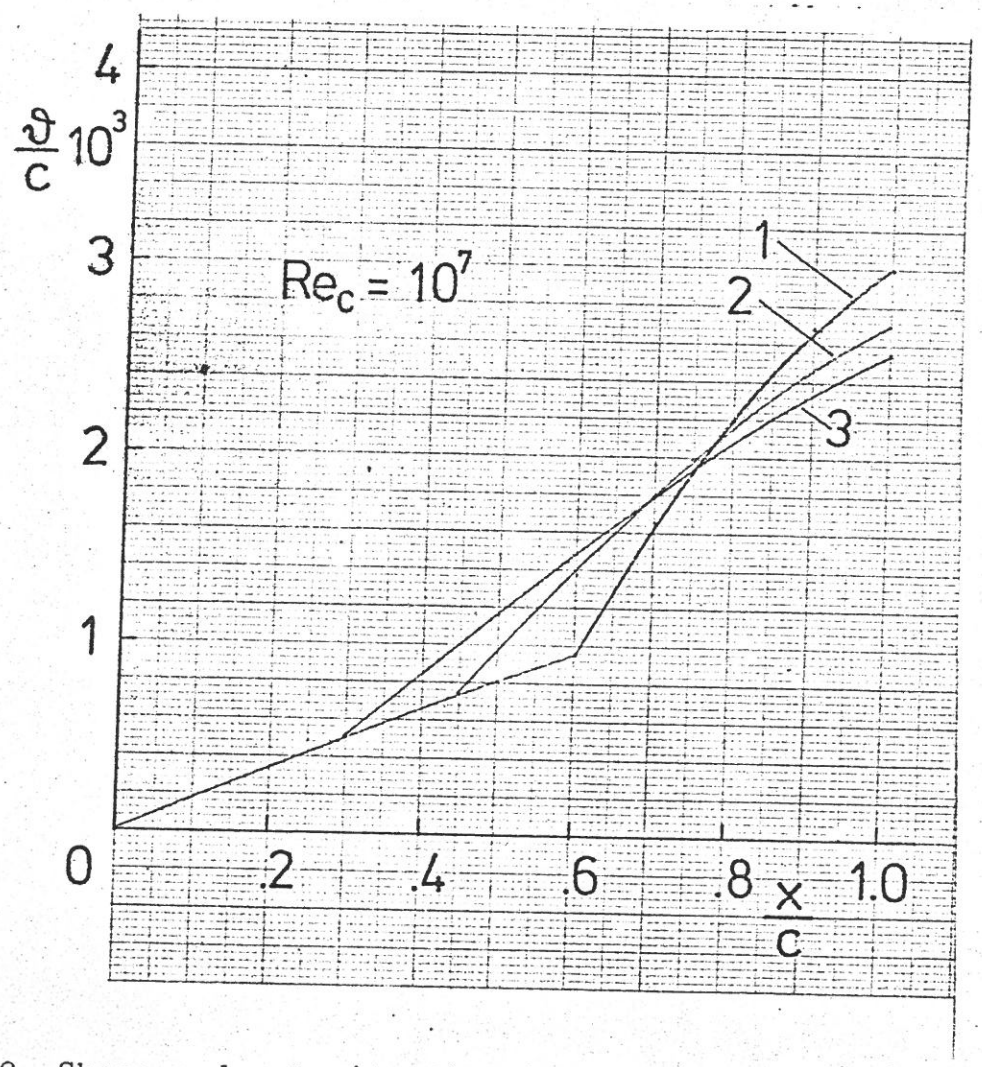

Fig. 49 Shape and velocity distribution of three typical airfoils. Boundary layer results for $\frac{x_T}{c} = .05$ and $Re_c = 10^7$

g) Airfoils with fixed transition

In the design of a wing not only airfoil aerodynamics but also structural and economic reasons establish the standard of surface quality. With other words, some sort of roughness fixes the transition position. Can an airfoil be adapted to such conditions, say for $M_\infty < .65$? One example may help to illustrate the possibilities.

Fig.51 shows a 17% thick airfoil for which it is assumed that transition takes place by some structural roughness at $\frac{x_T}{c} = 20\%$. In front of this roughness the velocity gradients are large enough to certify a laminar boundary layer for $Re_c \leq 3 \cdot 10^7$ and even for some lift variation. The drag values therefore will be considerably better than with a transition at $\frac{x_T}{c} \approx .08 \div .1$. The design lift coefficient is .75, a relatively high value because the drag at lift coefficients near zero is of no interest. Under cruising conditions the lift coefficient should be lower. With the help of an upward deflected flap the low drag bucket can be shifted down to c_L-values of around .3, according to the flight speed and wing loading. The high camber of the airfoil in front of the flap improves the high lift quality of the airfoil. Two further details will also improve the high lift and stall qualities of the airfoil:

At $\frac{x}{c} = 5\%$ there is a hidden velocity hump on the upper side which forms an instability range at high angles of attack and at $\frac{x}{c} = .67$ is another hump on the upper side to stop the trailing edge separation of the turbulent boundary layer. Both details are further explained in the next section. The velocity distribution in the region of the flap hinge is not developed because such details depend on the size and type of the flap.

Such airfoils may be useful for the general aviation.

h) Maximum lift of airfoils

Any single element airfoil reaches its maximum lift at about 15° angle of incidence, if we take reference to the zero lift direction.

As long as the Kutta-Joukowsky condition at the trailing edge is more or less satisfied, the nose region will develop high velocity

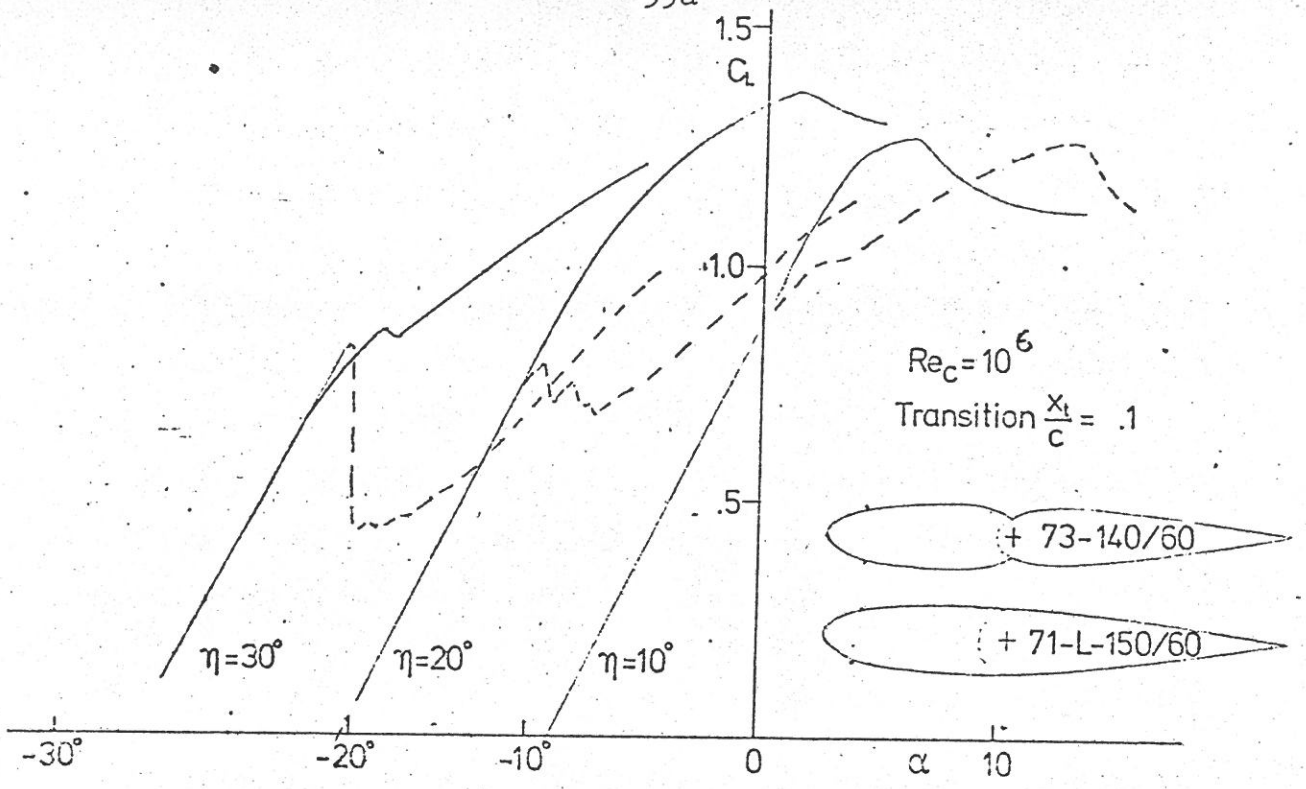

Fig.50 Comparison of $c_L(\alpha)$ for two airfoils with a 60 % flap and different flap setting at $Re_c = 10^6$. Transition at $\frac{x_t}{c}$ = .1
Full lines: bottle shaped FX 73-140/60

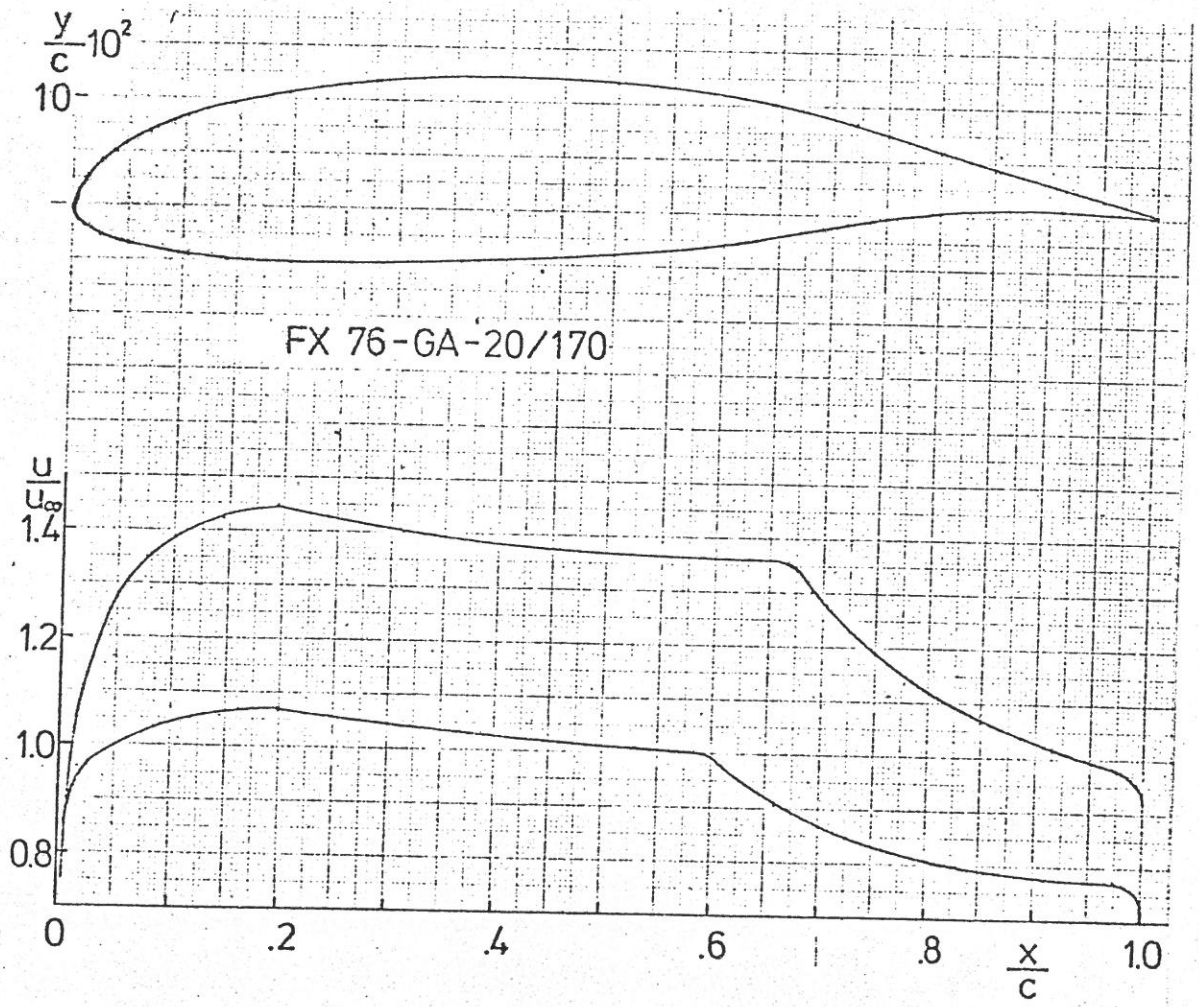

Fig.51 Shape and velocity distribution of an 17 % thick airfoil for an assumed transition position at $\frac{x_t}{c}$ =0.2

peaks and steep adverse pressure gradients. In general, this occurs in the first few percent of the chord and the boundary layer will be laminar and form a separation bubble. The steepness of the overall gradient causes a large separation angle, which spoils the initial thickness of the turbulent boundary layer. The type of pressure distribution downstream the bubble is clearly a concave one which, as can be seen from Fig.10, will react very favorable if we can improve the initial thickness of the turbulent boundary layer.

A suitable, but not an oversized roughness may do it. Better seems the concept of an instability range, to give the laminar boundary more space or time to develop its instability before it separates.

Fig.52 and Fig.53 illustrate this point. The blunt nosed airfoil can realize 20% more maximum lift than the NACA 0012 airfoil due to the better transition control. The test Reynoldsnumber $Re_c = 1 \div 3 \cdot 10^6$ is not high enough to produce transition at the edge of the pressure rise. Despite this inability the lift difference is large enough to be conclusive. Fig.54 shows the bubble and transition of both airfoils.

For the thin symmetrical airfoil the blunt nose produces also at low angles of incidence velocity peaks and transition near the nose. With a free transition this airfoil therefore has more drag than the NACA 0012. However, for a fixed transition at 7% chord the drag difference will disappear (see fully turbulent airfoils).

For thicker airfoils the same principle may be applied, but now the velocity peaks can be partly avoided. The airfoil of Fig.51 has this feature, but the laminar flow up to 20% chord is not disturbed by the hump at 7% chord.

The second principle to increase the maximum lift of single element airfoils applies for the turbulent boundary layer an extreme type of concave pressure distribution, which comes close to separation everywhere (Stratford distribution). This was first done by Liebeck and Ormsbee (18), see Fig.55.

Such designs strive for a high lift with a completely attached turbulent boundary layer on the upper side, which certainly can achieve high maximum lift . However, approaching this lift values

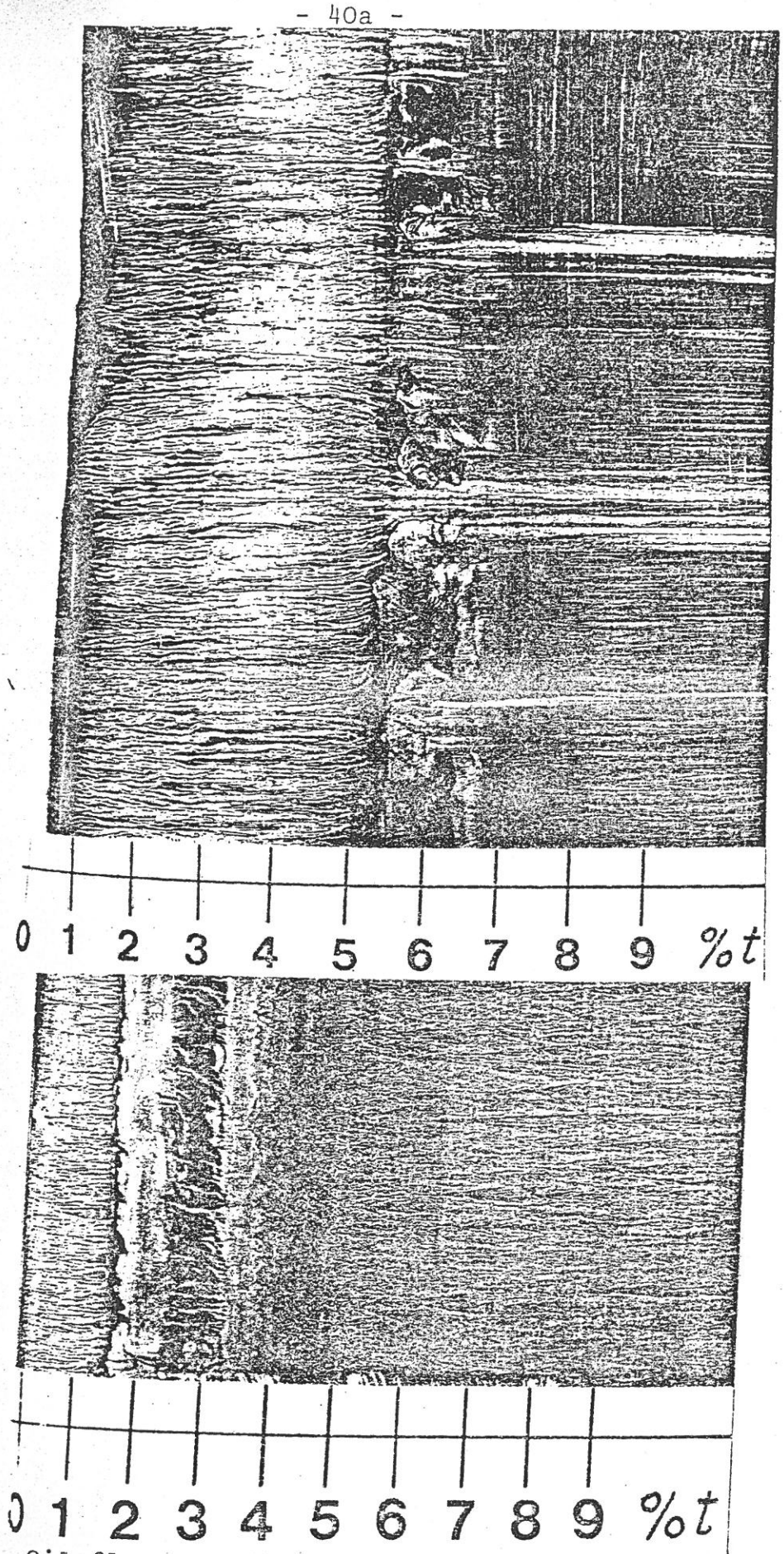

Fig.54 Oil flow near the nose ot the two airfoils of Fig.52 with instability range (upper picture) and without instability range (lower Picture). Numbers give the arc length in percent of chord.

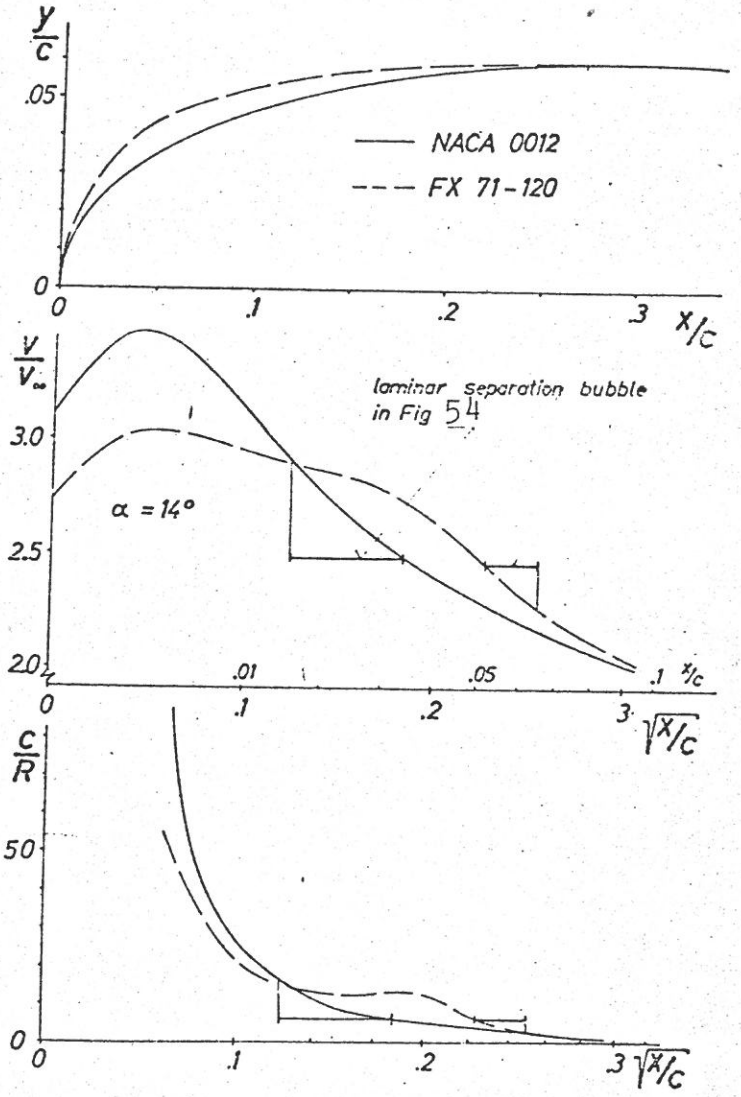

Fig. 52 Shape, velocity and curvature distribution of two airfoils with and without an instability range for the laminar boundary layer.

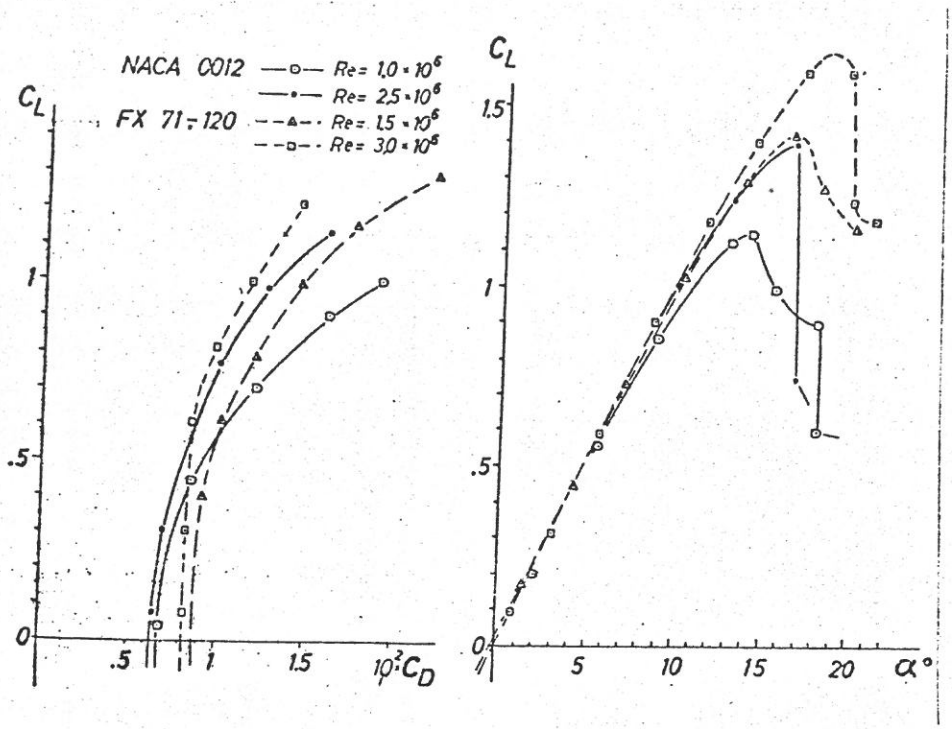

Fig.53a Drag and lift polare of the two airfoils of Fig.52. Re_c = 1.0 ÷ 3.0; transitionfree.

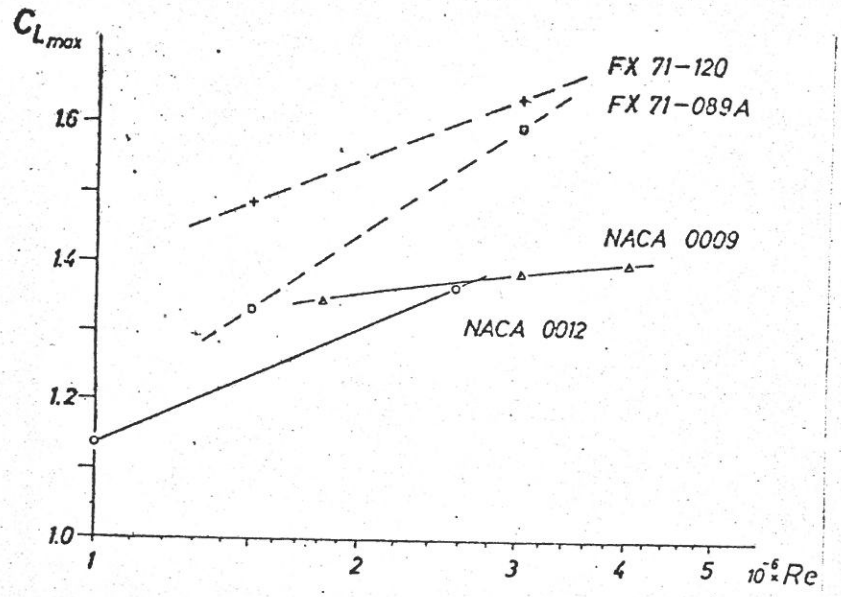

Fig.53b c_{Lmax} of two NACA airfoils and two FX modifications as function of Reynoldsnumber.

means also exhausting the boundary layer everywhere and the stall behaviour must be unacceptable, see Fig.56.

Similar lift coefficients may be reached by a careful transition control and applying high camber (19). Fig.57 gives an example where the camber in the last 40% of the upper surface is practically zero to avoid the influence on the turbulent boundary layer. The stall behaviour of this airfoil is a little better than in Fig.56.

Another possibility to increase the lift would be to increase the velocity at the trailing edge by a final thickness. If the trailing edge thickness is greater than about 0,2% it can be felt as a pressure drag increase. In certain cases, as for ships, the drag of the rudder may be unimportant and the trailing edge may be blown up to a square cut off trailing edge. The velocity here goes up and the same is allowed near the nose, as for the boundary layer only the ratio U_{TE}/U_1 is important. Therefore the suction force of such airfoils with thick trailing edges is enlarged. There are some interesting proposals to reduce the base drag of such airfoils (20).

In general, the maximum lift is intimately connected to a partly separated flow on the upper side. When this separation overrides the lift increase due to higher angles of incidence, we say the airfoil has stalled.

i) Stall behaviour

For low speeds and steady flow it is common place to distinguish the thin airfoil stall, the leading edge stall and the trailing edge stall. The first is associated to the phenomenon of the long separation bubble. The second follows, when the tiny laminar separation bubble explodes and the third type of stall is characterized by the slow upstream moving of the turbulent separation. It is the boundary layer behaviour which determines the stall. Therefore the same airfoil may show a leading edge stall at medium Reynoldsnumbers and trailing edge stall at higher Reynoldsnumbers.

It is not too difficult to change the leading edge stall with the sudden loss of lift into a trailing edge stall by means which have

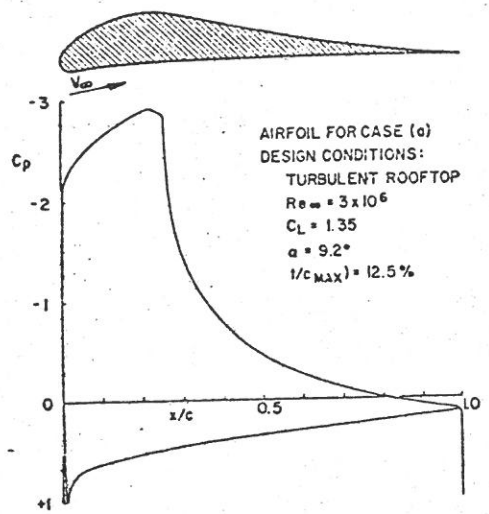

Figure 55 Airfoil design and theoretical pressure distribution for wind tunnel test, case (a).

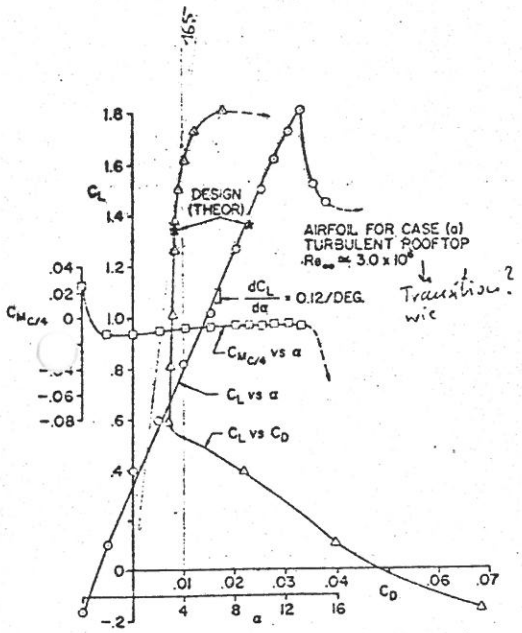

Figure 56a Experimental lift curve and drag polar, turbulent rooftop airfoil, case (a). Test conducted at $Re_\infty = 3 \times 10^6$.

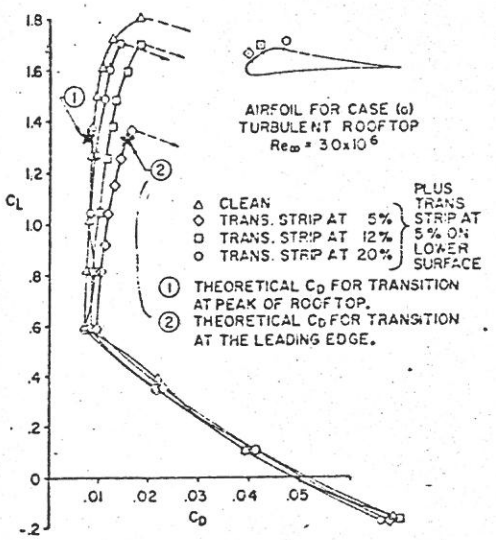

Figure 56b Experimental drag polars showing the effect of transition strips, turbulent rooftop airfoil, case (a).

been shown above in Fig.52 and 53. This however does not necessarily ensure a soft trailing edge stall, as Fig.53a also demonstrates.

The explanation is as follows:

Due to the shallow and short separation bubble higher angles of incidence are possible. In this special case the stall is a trailing edge stall, because the turbulent separation moves at $Re_c = 1.5 \cdot 10^6$ in a fast but steady manner to the midchord position. At the higher Reynoldsnumber the angle of incidence is three degrees higher, the laminar separation point now shifts suddenly from the 5% position to a 1% position. The initial conditions become worse and the highly loaded turbulent boundary layer can no longer stand the pressure gradient and the stall must become very abrupt.

This example illuminates the wellknown fact that small changes in the surface condition and hence the boundary layer state at the nose can have drastic effects near the maximum lift. Sometimes one wants designer, builders and users of aircraft would be more aware of this fact.

The most wanted quality at stall is a high lift, which doesn't change much up to 20 and more degrees. Obviously, some sort of bumper is necessary to counteract the ever increasing pressure peaks at the nose and to enable the boundary layer on the upper side to stay attached to about 2/3 of the chord.

An extended turbulent separation over the last third of the chord modifies the "fluid airfoil form" drastically and may redistribute the pressure distribution in the forward part to be acceptable for the boundary layer. In order to get a nearly constant total lift beyond the stall, it seems necessary, that the separation holds near the 70% chord position and only the separation angle changes at this position with the angle of incidence.

The separated flow acts as a flap which drastically unloads the velocity peaks at the nose. From Fig.31 we see that with a flap chord of 30% and a flap angle of 5° the lift change is $-\Delta c_L \approx .35$. With other words, such a flap reduces the lift from $c_L = 2.0$ to 1.65, when for instance the separation has started at this value. Fig.30 which holds for an unchanged position of the main airfoil has now to be applied with reversed signs i.e. the velocity peaks

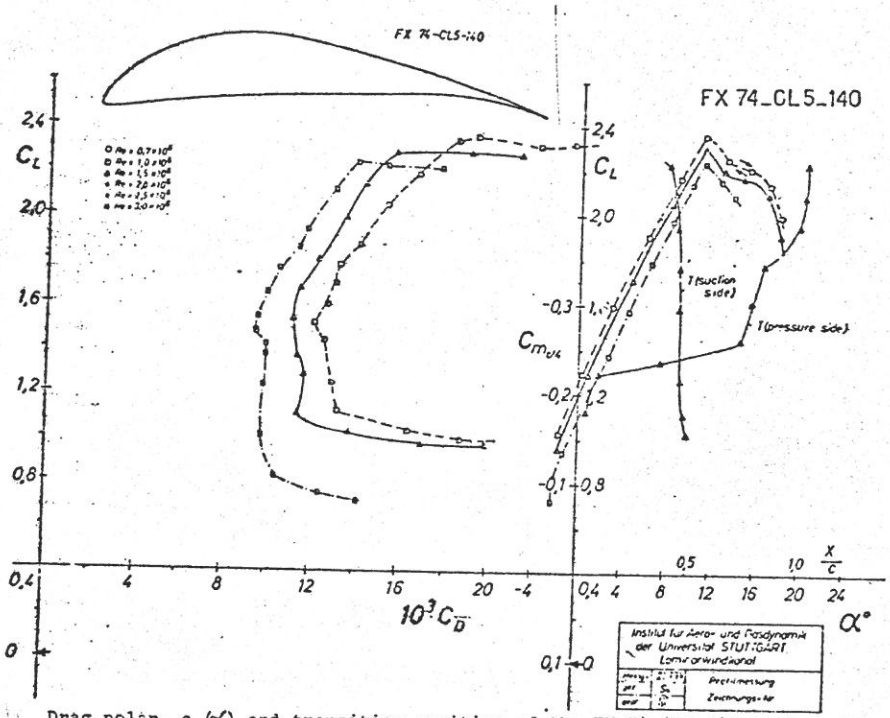

Drag polar, $c_L(\alpha)$ and transition position of the FX 74-CL5-140 at Reynolds-numbers of 1.0, 1.5 and $3.0 \cdot 10^6$.

Fig.57

due to the flap reduces the velocity peaks due to the angle of attack, and it is this effect which enables the boundary layer to stay attached beyond $C_{L\,max}$.

This behaviour of the "fluid" flap can be realized by two methods: the first investigates the development of the pressure distribution with separation and strives for a careful control of the transition near the nose region, which in turn has such a strong influence on the separation position.

The other method takes care of a high velocity hump on the upper side near the 70% position. Now at high angles of incidence the separation moves fast to this position, but stays there and is to some extent insensitive to the conditions at the nose.

Obviously, it is much easier to hit the wanted result of a constant $C_L = C_{L\,max}$ beyond the first stall with the second method than with the first one. The airfoil in Fig.51 is one example of a well proven principle.

Conclusions

Airfoil selection and airfoil design depend besides a clear defined set of desired qualities largely on the understanding of the environment under which the airfoil has to perform its task. The Reynoldsnumber and the Machnumber are the flow parameters, which are often so stringent that there remains not much to choose. In other cases, especially for Machnumbers below .7 and medium Reynoldsnumbers of 1÷20 millions, there is much freedom to adapt the airfoil also to other constraints as for instance surface construction, structural simplicity or weight and cost considerations. In such cases, the knowledge of the intimate interaction of airfoil shape, pressure distribution and boundary layer behaviour will help to judge the airfoil selection or to design a new one which may be better adapted to the wanted requirements.

References

(1) A.Walz — Strömungs- und Temperaturgrenzschichten, G.Braun, Karlsruhe 1966

(2) L.Rosenhead — Laminar Boundary Layers, Oxford University Press 1963

(3) H.Schlichting — Boundary Layer Theory, McGraw-Hill, New York

(4) R.Michel — Etude de la Transition sur les Profils d'Aile - Etablissement d'un Critère de Determination du Point de Transition et Calcul de la Traînée de Profil en Incompressible, ONERA Rapport 1/1578A, July 1951

(5) S.C.Wells — Effects of Freestream Turbulence on Boundary Layer Transition, AIAA Journ.5(1967), pp.172-174

(6) B.H.Carmichael, D.E.McNay — SUS Experimental Program Phase 2, NAA/MOG BHC-DEM-102(1963)

(7) F.X.Wortmann — Über den Ablösewinkel laminarer Ablöseblasen, DLR-FB 74-62, 1974

(8) A.M.O.Smith — Remarks on Fluid Mechanics of the Stall, AGARD-LS-74

(9) B.S.Stratford — The Prediction of Separation of the Turbulent Boundary Layer, J.Fluid Mech.5(1959), pp.1-16

(10) I.H.Abbott, A.E.v.Doenhoff — Theory of Wing Sections, Dover Publ.Inc., New York 1959

(11) F.X.Wortmann — Progress in the Design of Low Drag Airfoils, G.V.Lachmann,"Boundary Layer and Flow Control", Pergamon Press, London 1961

(12) F.W.Riegels — Aerodynamische Profile, R.Oldenbourg, München 1958, Butterworths, London 1967

(13) H.H.Pearcy — The Aerodynamic Design of Section Shapes for Swept Wings, Advances in Aeronautical Sciences, Vol.3-4 Pergamon Press, London 1962

(14) G.Y.Nieuveland, B.M.Spee — Transonic shockfree flow, fact or fiction? AGARD-CP 35, 1968

(15) F.X.Wortmann — Symmetrical Airfoils Optimized for Small Flap Deflection, Swiss, Aero-Revue 48(1973), p.147

(16) H.H.Pearcy, J.Osborne — Some Problems and Features of Transonic Aerodynamics, ICAS Congress 1970, Roma, Paper 70-14

(17) Th.E.Labrujere, W.Loeve, J.W.Slooff — An approximate method for the calculation of the pressure distribution on wing-body combinations at subcritical speeds, Paris 1968, AGARD-CP-71

(18) R.H.Liebeck — A Class of Airfoils Designed for High Lift in Incompressible Flow, J.of Aircraft, Vol.10(1973), p.610

(19) F.X.Wortmann — The Quest for High Lift, AIAA/MIT/SSA Symposium, Cambridge 1974, Paper 74-1018

(20) M.Tanner — New Investigations for Reducing the Base Drag of Wings with a Blunt Trailing Edge, AGARD-CP-124, 1973